ISTANBUL TECHNICAL UNIVERSITY ★ GRADUATE SCHOOL

YUKAWA-TYPE SCREENING INHERENT IN HIGHER DIMENSIONAL GRAVITY AND COSMOLOGY

Ph.D. THESIS

Ezgi YILMAZ

Department of Physics Engineering

Physics Engineering Programme

OCTOBER 2022

ISTANBUL TECHNICAL UNIVERSITY ★ GRADUATE SCHOOL

YUKAWA-TYPE SCREENING INHERENT IN HIGHER DIMENSIONAL GRAVITY AND COSMOLOGY

Ph.D. THESIS

Ezgi YILMAZ
(509182105)

Department of Physics Engineering

Physics Engineering Programme

Thesis Advisor: Prof. Dr. A. Savaş ARAPOĞLU

OCTOBER 2022

İSTANBUL TEKNİK ÜNİVERSİTESİ ★ LİSANSÜSTÜ EĞİTİM ENSTİTÜSÜ

YÜKSEK BOYUTLU KÜTLEÇEKİM VE KOZMOLOJİ ÇERÇEVESİNDE YUKAWA TİPİ DAVRANIŞIN İNCELENMESİ

DOKTORA TEZİ

Ezgi YILMAZ
(509182105)

Fizik Mühendisliği Anabilim Dalı

Fizik Mühendisliği Programı

Tez Danışmanı: Prof. Dr. A. Savaş ARAPOĞLU

EKİM 2022

Ezgi YILMAZ, a Ph.D. student of ITU Graduate School with ID number 509182105, successfully defended the thesis entitled "YUKAWA-TYPE SCREENING INHERENT IN HIGHER DIMENSIONAL GRAVITY AND COSMOLOGY", which she prepared after fulfilling the requirements specified in the associated legislations, before the jury whose signatures are below.

Thesis Advisor :	**Prof. Dr. A. Savaş ARAPOĞLU** Istanbul Technical University	.....
Jury Members :	**Prof. Dr. Kazım Yavuz EKŞİ** Istanbul Technical University	.....
	Prof. Dr. Neşe ÖZDEMİR Istanbul Technical University	.....
	Prof. Dr. Vedat Nefer ŞENOĞUZ Mimar Sinan Fine Arts University	.....
	Doç. Dr. A. Nihan KATIRCI Doğuş University	.....

Date of Submission : 30 September 2022
Date of Defense : 19 October 2022

FOREWORD

Firstly, I would like to thank Prof. A. Savaş ARAPOĞLU for the invaluable guidance and support that he has provided throughout my academic journey. He has always been truly encouraging, patient, and understanding, which helped me achieve so much more than I considered possible. I appreciate all that I have learned from him and look forward to learning more in years to come.

I am grateful to Dr. Maxim EINGORN, first, for the considerable amount of time he spent while helping me get a better understanding of the problems we have worked on and improve my research skills, which have reached a completely new level within the past couple of years. Secondly, for his genuine support, guidance and friendship, for the post-apocalyptic action plans and last but not least, for having introduced me to Randy O., a true inspiration to our generation.

I would like to express my gratitude to Prof. Alexander ZHUK for his continuous support and the interesting problems we have worked on, which led to some nice results presented in this thesis.

October 2022

Ezgi YILMAZ
(Scientist)

TABLE OF CONTENTS

Page

ABBREVIATIONS

ΛCDM	**:** Lambda-Cold Dark Matter
EoS	**:** Equation of State
ISL	**:** Inverse-Square Law
GR	**:** General Relativity
KK	**:** Kaluza-Klein
EMT	**:** Energy-Momentum Tensor
FRW	**:** Friedmann-Robertson-Walker
Her-CrB	**:** Hercules-Corona Borealis Great Wall
GW	
CMB	**:** Cosmic Microwave Background

SYMBOLS

$g^{\mu\nu}$	:	Metric tensor
δg^{ik}, h^{ik}	:	Metric tensor perturbations
c	:	Speed of light
G_N	:	Newtonian gravitational constant
η	:	Conformal time
t	:	Cosmic time
$\delta_{\alpha\beta}$	:	Kronecker delta
a	:	Scale factor
T^{ik}	:	Energy-momentum tensor
ε	:	Energy density
p	:	Pressure
u^k	:	Four-velocity
$\tilde{v}^\alpha$	:	Coordinate velocity
Π^{ik}	:	Stress tensor
G^{ik}	:	Einstein tensor
H	:	Hubble constant
a	:	Scale factor
z	:	Redshift
Φ, Ψ	:	Bardeen potentials
B^α	:	Vector potential
δ	:	Energy density contrast
ν	:	Velocity potential
ω	:	Equation of state parameter
c_s	:	Speed of sound
k	:	Comoving wave number
ρ	:	Rest-mass density
λ_{eff}	:	Effective screening length
Λ	:	Cosmological constant
S_D	:	$D-$dimensional total solid angle
$G_{\mathcal{D}}$	:	$\mathcal{D}-$dimensional gravitational constant
R^{ik}	:	Ricci tensor
R	:	Scalar curvature

LIST OF TABLES

Page

LIST OF FIGURES

Page

YUKAWA-TYPE SCREENING INHERENT IN HIGHER DIMENSIONAL GRAVITY AND COSMOLOGY

SUMMARY

At the intersection of gravitation and cosmology, a study of the large-scale structure of the Universe, and particularly, the search for a general relativistic scheme appropriate for formulating structure formation at all-scales makes up the principle objective of this thesis. Given the shortcomings of the Newtonian cosmological approximation at large scales, it appears inconvenient to keep employing Newtonian equations of motion in N-body codes of cosmological simulations, especially now when the upcoming surveys are promising high-precision scans of regions ever approaching the Hubble-scale. As the linear (relativistic) perturbation theory fails to describe gravitational interactions in the nonlinear regime, it is quite interesting to work on a scheme that incorporates the essential relativistic effects at large-enough regions, but also works well below the scale of nonlinearity.

The present work initially introduces a scheme that combines the characteristics of such an approach, namely, the *cosmic screening approach* towards all-scale cosmological perturbations, with the screening of gravity emerging through a distinct mechanism as part of the relativistic perturbation theory. Subsequently, it presents an effective screening length (the effective interaction range of Yukawa gravity) for gravitational interactions at cosmological scales, which matches the size of the largest-yet-observed cosmic structure, and thereby, argues for homogeneity and isotropy in the Universe not from few hundred megaparsecs, but from a few gigaparsecs on. The analysis is first carried out for the flat ΛCDM model, but later it is extended to involve curved spaces with the same energy components. The role of peculiar velocities, which is the key element in the developed scheme, is also investigated in detail beyond the scale of nonlinearity.

Elaborating further on Yukawa gravity in the cosmological framework, this thesis also presents a comparison of Newtonian approximation and Yukawa behaviour in terms of single particle gravitational force calculations performed in simulations of structure formation. Additionally, it investigates the impacts of periodicity on the Yukawa force to reveal the extent of deviations from the free-boundary problem. Apart from the N-body codes, which are generally run for cubic boxes replicated periodically in three dimensions, the motivation to study periodic boundaries also comes from theoretical grounds, from the fact that a multiply connected Universe (contrary to what is suggested by concordance cosmology, that is, the Universe is simply connected) would allow for flat space shaped as a finite-size three-torus. In this connection, the possible alternative expressions for the periodic gravitational potential and force have recently been studied in a comparative analysis in view of computational efficiency. With reference to the results therein, in the present work, the role of the effective screening length in the periodic formulation is discussed extensively to reveal that the associated effects are reduced for large-enough simulation boxes compared to the

screening length. On the other hand, small values of the interaction range to the box size ratio are also favoured by observational constraints on the considered topology, which place an upper bound of the order of 10^{-1} on the rescaled screening length in a cell with dimensions rescaled to unity.

Meanwhile, Yukawa potentials also emerge in higher dimensional Kaluza-Klein theories, albeit now as correction terms in metric coefficients.

Testing the compatibility of modified theories of gravity with gravitational tests performed in the solar system is an important part of evaluating their viability. In this connection, this thesis includes an extensive analysis of nonlinear $f(R)$ gravity in higher-dimensional space with spherical compactification of extra dimensions, where some nonlinear perfect fluid is considered to be the matter responsible for the curved background.

First, metric corrections are derived in the weak field limit, which acquire the form of two summed Yukawa potentials subject to constraints form the inverse-square law experiments. Motivated by the fact that two distinct scalar degrees of freedom are inherent in nonlinear $f(R)$ models (the scalaron) and in multidimensional gravity (the gravexciton/radion) separately, the relationship between these and the Yukawa masses emergent in the obtained metric corrections for several limiting cases are investigated. Additionally, constraints on the free parameters of the model are introduced and the formulas relating the four- and multi-dimensional gravitational constants to one another are presented so that an agreement with solar system experiments is reached and that the gravitational potential asymptotically tends to the Newtonian potential.

YÜKSEK BOYUTLU KÜTLEÇEKİM VE KOZMOLOJİ ÇERÇEVESİNDE YUKAWA TİPİ DAVRANIŞIN İNCELENMESİ

ÖZET

Kütleçekim ve kozmolojinin kesişiminde yer alan evrenin büyük ölçekteki yapısının, genel görelilik çerçevesinde, ufuk altı ve ufuk ötesi mesafelerde incelenmesi bu tezin başlıca amacını oluşturmaktadır. Yapı oluşumunu modelleyen kozmolojik simülasyonların birçoğu, hareket denklemlerini çözen N-parçacık kodlarında Newton yaklaşıklığına başvurmaktadır. Ancak gözlemsel çalışmaların günümüzde Hubble-ufkuna gittikçe yaklaşan mesafeler için gittikçe artan çözünürlükte veriler sundukları göz önünde bulundurulduğunda, kütleçekim hesaplarında kullanılan bu yaklaşıklık yetersiz kalır, çünkü bu formülasyon büyük ölçeklerde önem kazanan relativistik etkileri içermez. Öte yandan, relativistik pertürbasyon teorisi de küçük ölçeklerde, yani enerji yoğunluğundaki dalgalanmaların ortalama değere yaklaştığı mesafelerde geçerliliğini kaybeder. Kütleçekimsel etkileşimleri modellemek için bütün ölçeklerde etkin olan bir yaklaşım arayışı bu yönden oldukça ilginç bir problem olarak karşımıza çıkar.

Bu çalışmada, öncelikle, Hubble ufkunun altında ve ötesinde geçerliliğini koruyan *kozmik perdeleme yaklaşımı* ile relativistik pertürbasyon teorisinden türetilmiş bir diğer kütleçekimsel perdeleme mekanizmasını harmanlayan bir yöntem sunulmaktadır. Bu sayede, evrende gözlenmiş en büyük yapının boyutlarıyla tutarlı, Yukawa kütleçekiminin etkin etkileşim alanına karşılık gelen bir *etkin perdeleme mesafesi* türetilmiştir. Bu uzunluğun bugünkü değeri, evrenin homojen ve izotropik yapısının alt sınırını belirleyen ve literatürde daha önceki çeşitli çalışmalarda birkaç yüz megaparsec mertebesinde hesaplanan ölçeğin, birkaç gigaparsec mertebesinde olabileceğine işaret etmiştir. Başlangıç olarak ΛCDM modelinin öngördüğü düz uzay için geliştirilen model, sonrasında aynı enerji kompozisyonuyla eğri uzaylar, yani kapalı ve açık evrenler için genelleştirilmiştir. Homojen olmayan gravitasyonel alanın kaynağı olan parçacıkların hızlarının, söz konusu modelin önemli bir parçası olarak büyük ölçeklerde ihmal edilemeyecekleri gösterilmiştir.

Kozmik perdeleme yaklaşımında skaler potansiyel için birinci mertebeden alan denklemleri bir Helmholtz denklemi verir. Yeterince küçük ölçeklerde beklendiği üzere bu denklem, Newton potansiyelinin Poisson denklemine indirgenir. Büyük ölçeklerde ise Helmholtz denkleminin çözümü noktasal kütlelere ait Yukawa potansiyellerinin toplamı şeklinde bulunur. Buradaki Yukawa terimleri bir eşik uzaklığın üzerinde -ki bu da söz edilen perdeleme mesafesine karşılık gelir- gravitasyonel potansiyelin ve bunu takiben de kuvvetin, eksponansiyel olarak sönümlendiğine işaret eder. Alan denklemleri kullanılarak ede edilen bu sonuç, bu çerçevede relativistik bir etki olarak yorumlanmaktadır. Kütleçekim kuvvetinin belirli bir eşiğin üzerinde hızla etkisini kaybetmesi, kozmolojik yapılarının boyutlarına ait, etkileşim menziliyle karakterize bir üst sınırın varlığına işaret ederek, kozmolojik ilkenin öngördüğü, yeterince büyük ölçeklerde evrenin homojen ve izotropik olduğu

kabulünü desteklemektedir. Söz konusu yaklaşımdaki potansiyel ifadesinin bir diğer önemli özelliği de, birinci mertebedeki metrik pertürbasyonun sağlaması beklendiği üzere, konum üzerinden alınan ortalamasının sıfıra eşit olmasıdır.

Kozmolojik çerçevede perdeleme yaklaşımından gelen kütleçekimin Yukawa davranışı, yine tez kapsamında tek kaynak parçacığa ait alan ve kuvvet için, yapı oluşumu simülasyonlarıyla uyumlu bir kübik periyodik hücrede Newton yasasının davranışıyla karşılaştırılmıştır. İlgili bağıl farkın hücrenin yüzde birinden daha küçük bir mesafede 10^{-5} mertebesine geldiği, ve maddenin dominant olduğu, yapı oluşumuyla karakterize daha erken evrelere gidildikçe aynı bağıl farkın kaynak parçacığa daha da yaklaştığı görülmüştür.

Simülasyonlarda kullanılan N-parçacık kodlarının haricinde periyodik problem üzerinde çalışma motivasyonu evrenin çoklu-bağlantılı olabileceğinden de gelmektedir. Böyle bir evrende, sonlu boyutları olan üç boyutlu bir torus da düz uzaya karşılık gelebilir. Bu bağlamda, kozmik perdeleme yaklaşımının karakteristik denklemi olan gravitasyonel potansiyele ait Helmholtz-denklemi literatürde kübik torus topolojisi için çalışılmış, çözüme ait alternatif potansiyel ve potansiyelden türetilmiş kuvvet ifadeleri, nümerik hesaplamalarda sağlayacakları performanslar bakımından incelenmiştir. Periyodik sınır koşullarında başlangıçta simülasyon hücresinin merkezinde bulunan kaynak parçacık için bulunan çözümler, süperpozisyon ilkesiyle hücre içinde rastgele yerleştirilmiş parçacıklar için de genelleştirilebilmekte, bu bağlamda da N-parçacık simülasyonlarıyla uyumlu bir formülasyona izin vermektedirler. Karşılaştırılan ifadelerden kaynak parçacık ve periyodik görüntülerine ait Yukawa potansiyellerinin toplamından oluşan çözüm, gözlemsel limitlerle uyumlu on ve yüz gigaparsec mertebesindeki hücreler için en iyi sonuçları vermektedir. Kozmolojik simülasyonlarda sıklıkla kullanılan bugün 1 gigaparsecten küçük hücrelerde ise Yukawa potansiyellerinin Ewald toplamları şeklinde ifade edilen çözüm daha üstün performans sergiler. Bunlar göz önünde bulundurulduğunda Yukawa kuvvetinin etkin perdeleme mesafesinin periyodik formülasyondaki rolünü incelemek önem kazanmaktadır. Bu tez kapsamında da periyodik sınırların Yukawa kuvveti üzerindeki etkisi incelenmiş ve simülasyon hücresinin boyutları etkin perdeleme mesafesine kıyasla yeterince büyük tutulduğunda, bu etkilerin zayıfladığı belirlenmiştir. Yine tek kaynak parçacık için, periyodik sınırları olan kübik hücrede, periyodik ve serbest sınır koşullarında hesaplanan kuvvetlere ait bağıl farkın seçilmiş bazı sabit değerlerinin, gittikçe küçülen etkin perdeleme mesafesi için hücre içerisinde kaynak parçacıktan uzaklaştığı gösterilmiştir.

Kozmik perdeleme yaklaşımı, başlangıçta, metrik pertürbasyonların kaynağı delta fonksiyonlarıyla ifade edilen noktasal, relativistik olmayan kütleler olacak şekilde ortaya atılmış, literatürdeki çeşitli çalışmalarda lineer ve lineer olmayan ideal akışkanlar için genelleştirilmiştir. Ne var ki ikinci durumda akışkanların enerji yoğunluğu kontrastlarının her yerde küçük olduğu kabul edilmiştir. Bu çalışmada ise birinci-mertebede alan ve korunum denklemleri, en baştan lineer olmayan akışkanların da yoğunluk kontrastları gelişigüzel büyüklükte değerler alabilecek şekilde yazılmış ve skaler ve vektör potansiyelleri için Helmholtz denklemleri elde edilmiştir. İvmelenerek genişlemeyi Chaplygin gazı gibi modellerle açıklayan çalışmalara ait kozmolojik simülasyonlarda kullanılabilecek tam bir formül seti sunulmuştur.

Yukawa potansiyelleri yüksek boyutlu gravitasyon teorilerinde metrik pertürbasyonlarına gelen düzeltme terimleri olarak da karşımıza çıkmaktadır. Alternatif gravitasyon

teorilerinin Güneş sistemi testleriyle olan uyumluluğunu sınamak, geçerliliklerini test etmede önemli bir aşama teşkil etmektedir. Bu tez kapsamında da kompakt ekstra boyutların 2-boyutlu küre seçildiği yüksek boyutlu uzayda lineer olmayan $f(R)$ modelleri incelenmiştir. Arka plandaki uzayın eğriliği lineer olmayan bir ideal akışkan ile sağlanmıştır.

Çalışılan modeldeki homojen arka plan noktasal bir kütle ile pertürbe edilmiş ve metrik düzeltmelerin zayıf gravitasyonel alan limitinde iki Yukawa potansiyelinin toplamı şeklinde çözümleri olduğu gösterilmiştir. Lineer olmayan $f(R)$ modelleri ve yüksek boyutlu kütleçekime ait iki ayrı skaler serbestlik derecesi (sırasıyla skalaron ve radyon kütleleri) bulunduğundan bu ikisi ile metrik düzeltme terimlerindeki Yukawa kütleleri arasındaki ilişki bazı limit durumlar için araştırılmıştır. İncelenen durumlar özelinde, yüksek boyutlu kütleçekim sabiti için Newton kütleçekim sabiti ile modelin serbest parametreleri cinsinden ifadeler türetilmiştir. Yukawa potansiyeli için ters kare yasası deneylerinden gelen kısıtlamalar göz önünde bulundurularak $f''(R_0) = 0$ durumunda Güneş sistemi testleriyle uyumluluk için Yukawa kütlesi yeterince büyük olursa, ki bu yüksek boyutla ilişkili radyon kütlesine karşılık gelmektedir, noktasal kütlenin hal denklemindeki ek uzaya ait Ω parametresinin rastgele seçilebileceği, aksi durumda ise, yani rastgele büyüklükteki Yukawa kütlesi için bu parametrenin $\Omega = -1/2$ olması gerektiği gösterilmiştir.

1. INTRODUCTION

1.1 Introduction

In the cosmological setting and the framework of cosmic screening approach, Yukawa behaviour comes into play as the principal form of interaction between gravitating sources. The cosmic screening approach is originally based on the scheme of discrete cosmology and relies on the theory of general relativity (GR) together with the concordance (ΛCDM) model of cosmology [1]. Here, in the weak-field limit, the sources of small metric corrections are considered to be mass density fluctuations associated with point-like bodies. The mass density is handled in a non-perturbative manner so that the density contrast may exceed unity in small scales characterized by nonlinear dynamics. From the linearized Einstein equations, one obtains a Helmholtz-type equation for the gravitational potential which admits a solution containing summed Yukawa-terms associated with discrete particles that represent galaxies, clusters etc. For small enough regions, the equation is reduced to the Poisson equation for the Newtonian potential and at large cosmological scales, gravitational interaction undergoes exponential cutoff, conveniently prohibiting further growth of individual structures as expected in view of the cosmological principle.

As stated above, the cosmic screening approach, i.e. Yukawa-type screening of gravity in the cosmological setting, was introduced in [1], initially within the scheme of discrete cosmology, where sources of the inhomogeneous gravitational field were considered as discrete delta-shaped nonrelativistic bodies. Later, it was generalized to models containing perfect fluids [2, 3, 4, 5], to curved space [6], nonlinear f(R) gravity [7] and the phantom braneworld model [8]). Subsequently, with particular attention to the role of peculiar motion at large scales, it was combined with the screening mechanism proposed in [9] within the relativistic perturbation theory, which led to the derivation of an effective screening length [10], interpreted as the upper limit for the possible dimensions of an individual cosmic structure. Again, the scheme was

revisited for curved spaces [11] as well as for periodic boundaries [12, 13, 14] that are essential to simulations of structure formation [15, 16, 17, 18].

On the other hand, higher dimensional Kaluza-Klein (KK) theories [19, 20], investigated in their weak-field limit, exhibit the property that for nonlinear $f(R)$ models [21, 22, 23, 24, 25, 26] with flat background as well as for linear models with certain curved background geometries, metric perturbations introduced by a delta-shaped/compact gravitating source admit corrections in the form of the Yukawa potential[27, 28, 29, 30, 31]. Though negligible at distances much larger than the interaction range, in each case these terms reflect the additional scalar degree of freedom inherent in the theory, through the Yukawa mass, which indeed corresponds to the scalaron [22, 32, 33] and the radion [34, 35] mass, respectively. The additional degree of freedom in the first type of models emerges as a characteristic feature of $f(R)$ gravity whereas in the latter case, it relates to variations in the internal space volume. In all mentioned models, compactness of the d-dimensional internal space of the background manifold $M = M_4 \times M_d$ is required in order to recover the Newtonian potential far enough from the massive body.

In nonlinear $f(R)$ models, implementing the solutions for the perturbed metric coefficients in the three-dimensional space, i.e. setting $d = 0$, and considering a compact gravitating source with dust-like equation of state (EoS), it becomes possible to place constraints on the free parameters of the model [27]. The inverse square law (ISL) experiments set upper bounds for the Yukawa contribution to the gravitational potential [36]; so revealing the explicit expression for such corrections in terms of the free parameters, one may restrain their values. Straightforwardly, this allows to compare the largest possible range of Yukawa interaction to distances relevant to the gravitational tests in the solar system. A negligible correction term then means that the theory, in its weak field limit, behaves in the same way as GR [37, 38, 39, 40]. On the other hand, investigating cases where $d \neq 0$, one considers the asymptotic regions where the exponential function in the Yukawa term is either vanishing, or equal to unity [28]. As is typical of an astrophysical object, the gravitating source is assigned dust-like EoS in the three-dimensional external space and the EoS in the internal space is constrained by imposing the requirement that in these regions, the gravitational potential tends to the Newtonian potential.

Linear KK models of type $\mathbb{R} \times \mathbb{R}^3 \times S^d$, i.e. in which the internal space is described by a d-dimensional sphere, naturally admit the presence of some background fluid, responsible for the curved geometry of the spatial background. Introducing a source with the properties defined in the previous case, one reveals that the gravitational potential again acquires a Yukawa correction, subject to restrictions from the ISL experiments [29, 31]. Then, given the form of the correction term, constraints from experiments in the solar system may be satisfied either for a sufficiently large Yukawa mass, or by fine-tuning of the EoS parameter of the gravitating source in the internal space [29, 30, 31].

In the context of multidimensional KK models, the weak-field limit of linear gravity with spherical compactification of the internal space was studied in [29, 30, 31, 41, 42]. The more general nonlinear $f(R)$ models were investigated in [27, 28], where a flat internal space was assumed and hence, extra dimensions were toroidally compactified instead. For both classes of models, the linearized field equations were solved for the perturbed metric coefficients to reveal that they admit correction terms with Yukawa potentials. Then, viability of the models were investigated in view of experimental constraints from tests of gravity in the solar system.

1.2 Purpose of Thesis

This thesis aims to further investigate the Yukawa behaviour of gravity both in the higher dimensional setting and in the context of cosmological perturbations.

First, within the cosmic screening approach, the effective screening length will be derived, and the role of peculiar velocities will be explored at scales beyond the scale of nonlinearity. Curved spaces will also be considered for completeness. The formulation will be generalized to the case in which metric perturbations are sourced by energy density fluctuations of nonlinear perfect fluids that are not necessarily small. Still based on the cosmic screening approach, gravitational interactions will be studied in the periodic domain in view of the relationship between the extent of deviations from the free-boundary force and the effective screening length. With respect to single particle force calculations in cosmological simulations, Yukawa and Newtonian behaviours will be compared in cubic boxes with periodic boundaries.

Then, within the context of higher dimensional $f(R)$ gravity, the KK model with spherical compactification of the internal space and with some nonlinear prefect fluid as the background matter will be investigated. Introducing a delta-shaped gravitating source, perturbed metric coefficients will be studied in the weak field limit to see whether they receive Yukawa-type corrections in such setting. Concurrently, the viability of the model will be assessed based on the resulting form of the gravitational potential.

2. OVERTURE

2.1 Notation

Throughout the manuscript, the spacetime coordinates x^k, $k = 0, 1, 2, 3$, are marked by Latin indices (except in Chap. (7) they run from 0 to an arbitrary number D of spatial dimensions) and spatial vectors x^α are marked by Greek indices, or in certain contexts by boldface symbols such as $\mathbf{B}$ or $\mathbf{r}$. Partial derivatives ∂/∂_ν are denoted by ∂_ν. Symbols such as the prime, the dot etc. are used in different meanings is different contexts, therefore, each time they appear in text their roles are specified explicitly.

Einstein notation with repeated indices is used for demonstrating summations of vectors and tensors. Everywhere in the text the metric is represented by g^{ik} and the signature is $(+, -, -, -)$. In the context of cosmological perturbations, the metric perturbation is denoted by δg^{ik} whereas in the last chapter, for higher dimensional gravity, it is denoted by h^{ik}.

The speed of light c, together with constants such as the Newtonian gravitational constant G_N, are shown explicitly wherever necessary.

2.2 A Crude Review of the Relativistic Perturbation Theory

Rooted in the *Copernican principle*, arguing for the absence of special observes in physics, cosmological studies conventionally rely on the hypothesis that over large-enough distances, the universe is homogeneous and isotropic. Namely, it appears isotropic about all points [43, 44]. This is referred to as the *cosmological principle*. Though the statistical distribution of matter, i.e. of galaxies, favour a homogeneous pattern over large- enough scales [45, 46, 47, 48], the formation of cosmic structures themselves is associated with the growth of perturbations in the matter density, the information of which is contained in deviations from the homogeneous background.

Relativistic perturbation theory [49, 50] provides a solid framework for formulating perturbations at the linear level and at large scales; however, it breaks down when the density contrast approaches unity. Nonlinear dynamics relevant to later times are often modelled via Newtonian simulations, albeit with the drawback that Newtonian description of cosmological processes is insensitive to relativistic effects now.

2.2.1 The perturbed metric

In agreement with the cosmological principle, at the background level, the geometry of the homogeneous and isotropic Universe is described by the Friedmann-Robertson-Walker (FRW) metric

$$ds^2 = a^2\left(d\eta^2 - \delta_{\alpha\beta}dx^\alpha dx^\beta\right), \quad \alpha,\beta = 1,2,3, \tag{2.1}$$

for the particular case of flat space favoured by the ΛCDM model. Above and hereafter η represents the conformal time defined via $cdt = ad\eta$ (where c and t are the speed of light and the cosmic time, respectively), a is the scale factor and x^α stand for the comoving coordinates.

Introducing small perturbations about the background metric in (2.1), so that $g_{ik} = \overline{g_{ik}} + \delta g_{ik}$, $|\delta g_{ik}| \ll 1$, the line element of the inhomogeneous universe, in its most general form, may be expressed as

$$ds^2 = a^2\left[(1+2A)\,d\eta^2 - 2B_\alpha dx^\alpha d\eta - \delta_{\alpha\beta}\,(1+2C)\,dx^\alpha dx^\beta - 2h_{\alpha\beta}dx^\alpha dx^\beta\right], \tag{2.2}$$

where $A(\eta, x^\alpha)$ and $C(\eta, x^\alpha)$ transform as scalars, $B_\alpha(\eta, x^\alpha)$ as a 3-vector and $h_{\alpha\beta}(\eta, x^\alpha)$ as a rank-2 tensor under

$$x^{j\prime} = X^{j\prime}_k x^k, \quad X^{j\prime}_k = \begin{bmatrix} 1 & 0 \\ 0 & R^{\alpha\prime}_\beta \end{bmatrix}. \tag{2.3}$$

Here R^α_β is the rotation matrix satisfying $\delta_{\alpha\beta}R^\alpha_\gamma R^\beta_\tau = \delta_{\gamma\tau}$. The coordinate transformation described in (2.3) has the sought-for property that it preserves the symmetries of the background, i.e. it respects the slicing of spacetime into constant-time spacelike hypersurfaces with Euclidean metric [51].

Performing a scalar-vector-tensor decomposition, it is possible to split B_α into zero curl and zero divergence components, that yield a scalar B and a divergence-free vector $B^{(V)}_\alpha$:

$$B_\alpha = \partial_\alpha B + B^{(V)}_\alpha. \tag{2.4}$$

Similarly, the symmetric traceless tensor $h_{\alpha\beta}$ may be decomposed to obtain a scalar h, a divergence-free vector $h_\alpha^{(V)}$ and a symmetric traceless divergence-free tensor $h_{\alpha\beta}^{(T)}$:

$$h_{\alpha\beta} = \left(\partial_\alpha\partial_\beta - \frac{1}{3}\delta_{\alpha\beta}\triangle\right)h + \frac{1}{2}\left(\partial_\alpha h_\beta^{(V)} + \partial_\beta h_\alpha^{(V)}\right) + h_{\alpha\beta}^{(T)}\,. \tag{2.5}$$

By that means, the ten degrees of freedom in δg_{ik} shows in the four scalar, four vector and two tensor modes, which are separated into 2 physical + 2 gauge degrees of freedom for the scalar and vector perturbations.

In the first order, scalar vector and tensor perturbations may be studied separately in three distinct categories as the corresponding field equations are decoupled at this level. Scalar perturbations are coupled to the energy density and pressure contrasts through Einstein equations, and thus, structure formation in the universe is studied with respect to the evolution of these quantities. The remaining two scalar degrees of freedom in the perturbed energy-momentum tensor (EMT) are the velocity potential of irrotational flow and anisotropic stress, the latter being absent for perfect fluids. A, B, C and h, along with vector perturbations, vanish in the absence of matter. Only tensor modes survive in vacuum and they represent gravitational waves propagating across the homogeneous background. Vector perturbations, on the other hand, are associated with vorticity which decays quickly over time as the universe expands.

2.2.2 Longitudinal/conformal-Newtonian gauge

Perturbations introduced in the previous section depend on the choice of coordinates. Four of the ten degrees of freedom in δg_{ik} may be removed by gauge fixing, or by switching to gauge-invariant formalism [52, 53, 44] as these so-called *gauge degrees of freedom* merely correspond to perturbations in the coordinates with no physical correspondence.

Under the generic coordinate transformation $x^k \rightarrow x^{k\prime} \equiv x^k + \xi^k(\eta, x^\nu)$, where $\xi^k(\eta, x^\nu)$ is a first-order quantity, the set of functions below, the *Bardeen variables*, remain unchanged [52]:

$$\Phi \equiv A + \mathcal{H}(B - E') + (B - E')'\,, \quad \Psi \equiv -C - \mathcal{H}(B - E') + \frac{1}{3}\triangle E\,, \tag{2.6}$$

$$\zeta_\alpha \equiv h'_\alpha - B_\alpha^{(V)}\,, \quad h_{\alpha\beta}^{(T)}\,. \tag{2.7}$$

It is clear from (2.7) that the tensor mode $h_{\alpha\beta}^{(T)}$ is already gauge-invariant.

On *super-horizon* scales, working with gauge-dependent quantities appears cumbersome as it is difficult to clarify physical interpretations of perturbation variables. Even if the results obtained in a certain gauge may eventually be processed to meet observable quantities, there is also the possibility that gauge modes may provoke errors in numerical computations [54]. Nevertheless, there exists a particular gauge in which the two scalar fields A and C coincide with the Bardeen potentials in (2.6): $\Phi = A$ and $\Psi = -C$. It is the *conformal-Newtonian gauge* (also referred to as the *longitudinal gauge*) [49], with $\xi^0 = -B + E'$ and $\xi = E$. The scalar ξ is defined via $\xi_\alpha \equiv \partial_\alpha \xi + \xi_\alpha^{(V)}$. The off-diagonal scalars B and h vanish in this case (see Eqs. (2.33)-(2.39) of [44] for explicit expressions corresponding to the transformations of the full set of perturbation variables).

In the *sub-horizon* limit, where typical velocities are much smaller than the speed of light and general relativistic corrections are negligible (provided that the study is confined to the weak field limit), Φ corresponds to the Newtonian potential. Moreover, Φ and Ψ become identical to one another because the source of their difference, the anisotropic stress associated with the cosmic neutrino and microwave backgrounds of the early universe, becomes negligible here.

Taking into account scalar perturbations only, the line element in the conformal-Newtonian gauge may then be written as

$$ds^2 = a^2 \left[(1 + 2\Phi)\, d\eta^2 - \delta_{\alpha\beta} (1 - 2\Psi)\, dx^\alpha dx^\beta \right] . \tag{2.8}$$

For an all-inclusive treatment of metric perturbations, it is possible to resort to the *Poisson gauge* [54], which generalizes the longitudinal gauge by taking into account the vector and tensor modes as well.

2.2.3 Perturbations in the matter sector

The background EMT for perfect fluids has the generic form

$$\overline{T}^i_{\ k} = (\overline{\varepsilon} + \overline{p})\, \overline{u}^i \overline{u}_k - \overline{p} \delta^i_k \, , \tag{2.9}$$

where the energy density $\overline{\varepsilon}$ and pressure $\overline{p}$ are functions of time only, as implied by homogeneity. Given that $\overline{u}_k \overline{u}^k = 1$, the background four-velocity $\overline{u}_k = (a, 0, 0, 0)$ from (2.1) for the *comoving* observer.

Introducing perturbations in the matter sector, $T^i_k = \overline{T}^i_k + \delta T^i_k$, where now

$$T^i_k = (\varepsilon + p)\, u^i u_k - p\delta^i_k - \Pi^i_k \,, \tag{2.10}$$

and $u^i \equiv dx^i/ds$, the explicit expressions for the EMT components read

$$\begin{aligned} T^0_0 &= \overline{\varepsilon} + \delta\varepsilon \,, \\ T^0_\alpha &= -(\overline{\varepsilon} + \overline{p})\,(\tilde{v}_\alpha + B_\alpha) \,, \\ T^\alpha_\beta &= -(\overline{p} + \delta p)\,\delta^\alpha_\beta - \Pi^\alpha_\beta \,, \end{aligned} \tag{2.11}$$

up to first order. Unlike the average quantities, the energy density and pressure perturbations here, $\delta\varepsilon$ and δp, may depend both on time and position. The 3-vector $\tilde{v}_\alpha$ corresponds to the peculiar velocity (or, the *coordinate velocity*) defined as $\tilde{v}_\alpha \equiv dx^\alpha/d\eta$. Similar to (2.4), a decomposition of the form $\tilde{v}_\alpha = \partial_\alpha \tilde{v} + \tilde{v}^{(V)}_\alpha$ allows to introduce the *velocity potential*, the scalar $\tilde{v}$, of the irrotational flow. As for the stress tensor Π^i_k, it is possible to set $u^i \Pi_{ik} = 0$ (which implies $\Pi^0_0 = \Pi^0_\alpha = 0$) so that the only nonzero contribution comes from its spatial part - the traceless *anisotropic stress tensor*. It may also be decomposed into scalar, vector and tensor parts like the metric perturbation $h_{\alpha\beta}$:

$$\Pi_{\alpha\beta} = \left(\partial_\alpha\partial_\beta - \frac{1}{3}\delta_{\alpha\beta}\triangle\right)\Pi + \frac{1}{2}\left(\partial_\alpha \Pi^{(V)}_\beta + \partial_\beta \Pi^{(V)}_\alpha\right) + \Pi^{(T)}_{\alpha\beta} \,. \tag{2.12}$$

It is important to note that perfect fluids do not have anisotropic stress, and thereby, no tensor modes in the perturbed EMT.

Gauge degrees of freedom are also present in the EMT perturbations. There are four scalars, $\delta\varepsilon$, δp, $\tilde{v}$, and Π, two divergence-free vectors from $\tilde{v}_\alpha$ and Π^α_β, and a symmetric, divergence-free traceless 3-tensor from Π^α_β. Again, only six are physical. Given the way each variable transforms (see Eqs. (2.77)-(2.83) of [44] for the complete set of corresponding formulae) under the generic infinitesimal coordinate transformation introduced the previous section, one may obtain gauge-invariant quantities by combining matter perturbations with one another, and as well by combining those with metric perturbations (see Sect. (2.2.4) of [44]).

On the other hand, in the conformal-Newtonian gauge, the four scalars are

$$\delta\hat{\varepsilon} = \delta\varepsilon + \overline{\varepsilon}'\,(B - E') \,, \quad \delta\hat{p} = \delta p + \overline{p}'\,(B - E') \,, \quad \hat{v} = \tilde{v} + E' \,, \quad \hat{\Pi} = \Pi \,. \tag{2.13}$$

Despite the gauge-dependent formulation of perturbations here, the variables $\hat{\varepsilon}$ and $\hat{v}$, the energy density and velocity potential, respectively, acquire Newtonian characteristics in the sub-horizon limit, where the Bardeen potential Φ also coincides with the Newtonian gravitational potential.

All hatted quantities in (2.13) and in the rest of this chapter refer to perturbation variables expressed in the conformal-Newtonian gauge.

2.2.4 Scalar sector field equations in the conformal-Newtonian gauge

Substituted in *Einstein field equations* $G^i_k = \kappa T^i_k$ (see, e.g., Chap. (3) of [55] for a full derivation of the *Einstein tensor* G^i_k from the metric), Eqs. (2.1) and (2.9) yield the *Friedmann equations* governing the dynamics of the background universe:

$$\begin{aligned} \frac{3\mathcal{H}^2}{a^2} &= \kappa\overline{\varepsilon} \\ 2\mathcal{H}' &= -\frac{\kappa a^2}{3}\left(\overline{\varepsilon} + 3\overline{p}\right) . \end{aligned} \tag{2.14}$$

Here, as well as in the chapters that follow, $\mathcal{H} \equiv a'/a \equiv (da/d\eta)/a$, so that $\mathcal{H} = aH/c$, where H is the Hubble constant, and $\kappa \equiv 8\pi G_N/c^4$, where G_N stands for the Newtonian gravitational constant.

According to the ΛCDM model, the energy content of the universe today consists mainly of vacuum energy (the cosmological constant), followed by pressureless nonrelativistic matter in the form of cold dark matter (CDM) and baryons (the latter roughly equals 1/5 of the CDM density). Radiation contribution is negligible. The energy density $\overline{\varepsilon}$ and pressure $\overline{p}$ values in the above set, however, correspond to the added contribution of all species for the moment in order to present a general formulation of cosmic dynamics.

Going to first order and considering scalars only, $\delta G^i_k = \kappa \delta T^i_k$ yields [51]

$$\begin{aligned} \delta G^0_0 \quad &\rightarrow \quad \triangle\Psi - 3\mathcal{H}\left(\Psi' + \mathcal{H}\Phi\right) = \frac{\kappa}{2}a^2\delta\hat{\varepsilon}\,, \\ \delta G^0_\alpha \quad &\rightarrow \quad \partial_\alpha\left(\Psi' + \mathcal{H}\Phi\right) = -\frac{\kappa}{2}a^2\left(\overline{\varepsilon} + \overline{p}\right)\partial_\alpha\hat{v}\,, \\ (\mathrm{Trace}) \quad \delta G^\alpha_\beta \quad &\rightarrow \quad \Psi'' + \mathcal{H}\left(\Phi' + 2\Psi'\right) + \left(2\mathcal{H}' + \mathcal{H}^2\right)\Phi + \frac{1}{3}\triangle\left(\Phi - \Psi\right) \\ &\qquad = \frac{\kappa}{2}a^2\delta\hat{p}\,. \end{aligned} \tag{2.15}$$

from (2.8) and (2.11). The traceless piece of the δG^α_β equation has been omitted from the last expression. Converted to Fourier space, it reveals the relation $(\Phi - \Psi) \propto \Pi$

(see Sect. (10) of [51] for a detailed demonstration), which means, disregarding anisotropic stress, the two Bardeen potentials become identical:

$$\begin{aligned} \delta G^0_0 \quad &\rightarrow \quad \triangle\Phi - 3\mathcal{H}\left(\Phi' + \mathcal{H}\Phi\right) = \frac{\kappa}{2}a^2\delta\hat{\varepsilon}\,, \\ \delta G^0_\alpha \quad &\rightarrow \quad \Phi' + \mathcal{H}\Phi = -\frac{\kappa}{2}a^2\left(\overline{\varepsilon} + \overline{p}\right)\hat{v}\,, \\ (\text{Trace}) \quad \delta G^\alpha_\beta \quad &\rightarrow \quad \Phi'' + 3\mathcal{H}\Phi' + \left(2\mathcal{H}' + \mathcal{H}^2\right)\Phi = \frac{\kappa}{2}a^2\delta\hat{p}\,. \end{aligned} \tag{2.16}$$

Anisotropic stress is associated with free-streaming of relativistic species. Photons decouple from the cosmic plasma (at $z \sim 1000 - 1200$ [56]) already after the matter-radiation equality ($z \sim 3400$ [56]), i.e. when matter density begins to dominate, thus neglecting their contribution here is well justified. However, it is worth noting that neutrino decoupling takes place as early as $z \sim 6\times10^9$ [56], and one should beware of the problematic aspects of such a simplification from neutrinos' side, especially when high precision is targeted in calculations. Meanwhile, gradients of the scalars in the δG^0_α equation have been replaced by these functions themselves for spatial averages of perturbations vanish in the first-order.

2.2.5 Energy-momentum conservation

Assuming a perfect fluid and neglecting anisotropic stress in (2.11), still in the conformal- Newtonian gauge, energy-momentum conservation equations $\nabla_k T^k_i = 0$ follow as

$$\begin{aligned} i = 0 \rightarrow \quad (\text{Background}) \quad \overline{\varepsilon}' &= -3\mathcal{H}\left(\overline{\varepsilon} + \overline{p}\right), \\ i = 0 \rightarrow \quad (1^{\text{st}}\text{order}) \quad \hat{\delta}' &= \left(1 + \frac{\overline{p}}{\overline{\varepsilon}}\right)(3\Phi' - \triangle\hat{v}) + 3\mathcal{H}\left(\frac{\overline{p}}{\overline{\varepsilon}}\hat{\delta} - \frac{\delta\hat{p}}{\overline{\varepsilon}}\right), \\ i = \alpha \rightarrow \quad (1^{\text{st}}\text{order}) \quad \hat{v}' &= -\mathcal{H}\hat{v}\left(1 - 3\frac{\overline{p}'}{\overline{\varepsilon}'}\right) - \frac{\delta\hat{p}}{\overline{\varepsilon} + \overline{p}} - \Phi\,, \end{aligned} \tag{2.17}$$

with respect to the line element (2.8). The first-order *continuity equation* ($i = 0$) is expressed in terms of the energy density contrast, defined via $\hat{\delta} \equiv \delta\hat{\varepsilon}/\overline{\varepsilon}$. These equations also hold for each (non-interacting) species separately, once the corresponding EoS parameter $\omega \equiv \overline{p}/\overline{\varepsilon}$ is substituted. The $i = \alpha$ component of the conservation equation corresponds to the *Euler equation*.

It is worth noting that for adiabatic perturbations, the squared speed of sound $c_s^2 = \delta p/\delta\varepsilon = \overline{p}'/\overline{\varepsilon}'$.

2.2.6 Evolution of perturbations and structure growth

The sets of equations (2.16) and (2.17), together with the background Friedmann equations in (2.14), determine the evolution of perturbation variables.

When studying cosmological perturbations, *horizon* is defined as the time-dependent Hubble scale, i.e. $1/\mathcal{H}$. Expressed in Fourier space, the $k-$modes of perturbations that satisfy $k^{-1} \ll \mathcal{H}^{-1}$ correspond to *sub-horizon* scales and those for which $k^{-1} \gg \mathcal{H}^{-1}$, correspond to *super-horizon* scales. In the radiation-dominated and matter-dominated epochs, $\mathcal{H}^{-1} \propto a$ and $\mathcal{H}^{-1} \propto a^{1/2}$, respectively, and modes outside the horizon become sub-horizon modes in time as the physical wavelengths $\lambda_{\rm phys} \propto a$ fall behind $a\mathcal{H}^{-1}$.

Originated in the early universe, all modes of Φ and $\hat{\delta}$ that are outside the horizon are *frozen*, that is, $\Phi, \hat{\delta} = \text{const}$ (for $\omega = \text{const}$).

During the radiation-dominated period, sub-horizon modes of the metric perturbation Φ oscillate with decaying amplitude, and following the transition to the matter era, again, they remain constant.

On the other hand, throughout the radiation era, sub-horizon modes of the radiation density contrast $\hat{\delta}_r$ oscillate about the point $\hat{\delta}_{r-eq} = 0$ with constant amplitude. At this epoch, baryonic matter is tightly coupled to photons, and thereby, is affected by radiation pressure that prevents gravitational collapse. In other words, perturbations of the photon-baryon fluid oscillate inside the horizon, i.e. below the critical scale characterized by the *Jeans' length* $\lambda_J = c_s\sqrt{\pi/\left(G_N\overline{\varepsilon}\right)}$, until matter-radiation equality takes place at $z_{eq} = 3400$. In the matter era, perturbations in $\hat{\delta}_r$ keep oscillating with constant amplitude, only now about a shifted point $\hat{\delta}_{r-eq}$. Meanwhile, the speed of sound gets smaller to allow for the growth of perturbations and eventually, following recombination, baryonic matter gets trapped in the potential wells of the CDM density field. Dark matter density contrast $\hat{\delta}_C$, which grows $\propto \ln a$ during the radiation era, evolves $\propto a$ after z_{eq}. As fluctuations grow further to enter the nonlinear regime, the scheme of relativistic perturbation theory breaks down. The ongoing process of structure growth needs to be studied numerically from that point on.

An explicit mathematical demonstration of the above explained processes can be found in various references on cosmological perturbations. Some useful lecture notes with comprehensive narration include, e.g. [51, 56].

3. THE COSMIC SCREENING APPROACH

Cosmic screening approach, formulated within discrete cosmology, aims to describe gravitational interactions at all scales, from distances relevant to nonlinear dynamics to super-horizon cosmological scales.

The weak field limit of GR at sub-horizon scales admits Newtonian interaction between nonrelativistic bodies. Nonlinear dynamics relevant to small distances, where linear perturbation theory breaks down, is hence well described by the Newtonian cosmological approximation, which is often employed in N-body codes for modelling the growth of cosmic structures. The scheme of cosmic screening relies entirely on non-perturbative approach to the mass density. Therefore, at sub-horizon scales, the analytical expression for the scalar potential complies with the Newtonian approximation. Meanwhile, it also addresses also the question of how the form of gravitational interaction is altered at scales where the cosmological principle disfavours structure growth.

At large-enough scales, the gravitational force of the cosmic screening approach undergoes exponential decay. In other words, Yukawa-type screening of gravity comes into play to restrain interactions beyond the corresponding screening length. The underlying equations follow from GR and the ΛCDM model of cosmology, disregarding the contribution of relativistic species. As the scheme is based on discrete cosmology, inhomogeneous matter distribution is modelled via distinct point-like bodies, which represent pressureless nonrelativistic matter sources such as galaxies, groups of galaxies etc.

3.1 The Inhomogeneous Gravitational Field of Discrete Cosmology

The information of the inhomogeneous Universe, limited to the weak gravitational field limit and in the Poisson gauge, is contained in the perturbed metric [44, 52]

$$ds^2 = a^2 \left[(1 + 2\Phi)\, d\eta^2 + 2B_\alpha dx^\alpha d\eta - (1 - 2\Phi)\, \delta_{\alpha\beta} dx^\alpha dx^\beta \right] \tag{3.1}$$

in the absence of anisotropic stress. Functions $\Phi(\eta, \mathbf{r})$ and $B_\alpha(\eta, \mathbf{r})$ (satisfying $\nabla\mathbf{B} \equiv \delta^{\alpha\beta}\partial_\beta B_\alpha = 0$) are the first-order scalar and vector perturbations, respectively. Investigation of tensor modes in the first-order lies beyond the scope of this approach, hence the corresponding perturbation variable has been omitted in (3.1).

Subsequently, the linearized Einstein equations $\delta G^i_k = \kappa \delta T^i_k$ read

$$\triangle\Phi - 3\mathcal{H}\left(\Phi' + \mathcal{H}\Phi\right) = \frac{1}{2}\kappa a^2 \delta T^0_0\,, \tag{3.2}$$

$$\frac{1}{4}\triangle B_\alpha + \partial_\alpha\left(\Phi' + \mathcal{H}\Phi\right) = \frac{1}{2}\kappa a^2 \delta T^0_\alpha\,, \tag{3.3}$$

$$\Phi'' + 3\mathcal{H}\Phi' + \left(2\mathcal{H}' + \mathcal{H}^2\right)\Phi = 0\,, \tag{3.4}$$

$$\left(\partial_\beta\partial B_\alpha + \partial_\alpha\partial B_\beta\right)' + 2\mathcal{H}\left(\partial_\beta\partial B_\alpha + \partial_\alpha\partial B_\beta\right) = 0\,, \tag{3.5}$$

where the fluctuations of the matter EMT $\delta T^i_k \equiv T^i_k - \overline{T}^i_k$, are obtained from the tensor components [38, 57, 58]

$$T^{ik} = \sum_n \frac{m_n c^2}{\sqrt{-g}} \frac{dx^i_n}{d\eta}\frac{dx^k_n}{d\eta}\frac{d\eta}{ds_n}\delta\left(\mathbf{r} - \mathbf{r}_n\right)\,, \tag{3.6}$$

appropriate for a collection of discrete point-like nonrelativistic particles with masses m_n. In Eq. (3.6), $g \equiv \det[g_{ik}]$ and $\mathbf{r}_n$ indicates the comoving radius vector of the $n-$th particle. Metric corrections are sourced by fluctuations in the mass density $\delta\rho \equiv \rho - \overline{\rho}$, treated in a nonperturbative manner. Therefore, even though the smallness of Φ and B_α is an essential aspect, the condition $|\delta\rho| \ll \overline{\rho}$ is not imposed this approach. The rest mass density in the comoving coordinates is expressed as

$$\rho = \sum_n m_n \delta\left(\mathbf{r} - \mathbf{r}_n\right) = \sum_n \rho_n\,, \tag{3.7}$$

so arranging their right-hand sides (RHS) accordingly, Eqs. (3.2) and (3.3) may be cast into a set of Helmholtz equations for Φ and B_α, that are [1]

$$\frac{1}{4}\triangle\mathbf{B} - \frac{\kappa\overline{\rho}c^2}{2a}\mathbf{B} = -\frac{\kappa c^2}{2a}\left(\sum_n \rho_n \tilde{\mathbf{v}}_n - \nabla\Xi\right)\,, \tag{3.8}$$

$$\triangle\Phi - \frac{3\kappa\overline{\rho}c^2}{2a}\Phi = \frac{\kappa c^2}{2a}\delta\rho - \frac{3\kappa c^2\mathcal{H}}{2a}\Xi\,, \tag{3.9}$$

where

$$\Xi = \frac{1}{4\pi}\sum_n m_n \frac{\left(\mathbf{r} - \mathbf{r}_n\right)\tilde{\mathbf{v}}_n}{|\mathbf{r} - \mathbf{r}_n|^3}\,. \tag{3.10}$$

The auxiliary function Ξ, associated with the comoving peculiar velocities $\tilde{\mathbf{v}}_n$ of the particles, is introduced in order to facilitate the decoupling of equations for the scalar and vector perturbations. Eqs. (3.8) and (3.9) admit the solutions [1]

$$\begin{aligned}\mathbf{B} &= \frac{\kappa c^2}{8\pi a}\sum_n \left[\frac{m_n\tilde{\mathbf{v}}_n}{|\mathbf{r}-\mathbf{r}_n|}\cdot\frac{\left(3+2\sqrt{3}q_n+4q_n^2\right)\exp\left(-2q_n/\sqrt{3}\right)-3}{q_n^2}\right.\\ &+ \left.\frac{m_n\left[\tilde{\mathbf{v}}_n\left(\mathbf{r}-\mathbf{r}_n\right)\right]}{|\mathbf{r}-\mathbf{r}_n|^3}\left(\mathbf{r}-\mathbf{r}_n\right)\cdot\frac{9-\left(9+6\sqrt{3}q_n+4q_n^2\right)\exp\left(-2q_n/\sqrt{3}\right)}{q_n^2}\right],\end{aligned} \tag{3.11}$$

$$\begin{aligned}\Phi &= \frac{1}{3}-\frac{\kappa c^2}{8\pi a}\sum_n\frac{m_n}{|\mathbf{r}-\mathbf{r}_n|}\exp\left(-q_n\right)\\ &+ \frac{3\kappa c^2}{8\pi a}\mathcal{H}\sum_n\frac{m_n|\tilde{\mathbf{v}}_n\left(\mathbf{r}-\mathbf{r}_n\right)|}{|\mathbf{r}-\mathbf{r}_n|}\cdot\frac{1-\left(1+q_n\right)\exp\left(-q_n\right)}{q_n^2},\end{aligned} \tag{3.12}$$

for

$$\mathbf{q}_n\left(\eta,\mathbf{r}\right)\equiv\sqrt{\frac{3\kappa\overline{\rho}c^2}{2a}}\left(\mathbf{r}-\mathbf{r}_n\right),\quad q_n\equiv|\mathbf{q}_n|\,. \tag{3.13}$$

Owing to the form of (3.6), and for the metric introduced in (3.1), energy-momentum fluctuations to be substituted in the RHS of the linearized field equations (3.2)-(3.5), up to first-order, have the forms

$$\delta T_0^0=\frac{c^2}{a^3}\delta\rho+\frac{3\overline{\rho}c^2}{a^3}\Phi\,,\quad \delta T_\alpha^0=-\frac{c^2}{a^3}\sum_n\rho_n\tilde{v}_n^\alpha+\frac{\overline{\rho}c^2}{a^3}B_\alpha\,,\quad T_\beta^\alpha=0\,. \tag{3.14}$$

The terms $\propto\Phi,\mathbf{B}$ later contribute to the left-hand side (LHS) of Eqs. (3.8) and (3.9) for the scalar and vector potentials. In return, the solutions given in (3.11) and (3.12) admit exponentially decaying pieces, which hint at the Yukawa behaviour of these quantities.

The parameter q_n specifies the interaction range of Yukawa gravity via [1]

$$\mathbf{q}_n\left(\eta,\mathbf{r}\right)\equiv\frac{a\left(\mathbf{r}-\mathbf{r}_n\right)}{\lambda}\,, \tag{3.15}$$

where $\lambda\equiv\sqrt{2a^3/(3\kappa\overline{\rho}c^2)}$ represents the time-dependent screening length in the cosmological setting.

The Yukawa behaviour of gravitational interactions is also manifest in the equation of motion of individual particles, which are composed entirely of exponentially decaying

terms:

$$
\begin{aligned}
& (a\tilde{\mathbf{v}}_k)' = -a\left(\nabla\Phi|_{\mathbf{r}=\mathbf{r}_k} + \mathcal{H}\mathbf{B}|_{\mathbf{r}=\mathbf{r}_k}\right) \\
= & \sum_{n\neq k} -\frac{\kappa c^2}{8\pi}\left[\frac{m_n(\mathbf{r}-\mathbf{r}_n)}{|\mathbf{r}-\mathbf{r}_n|^3}\left(1+q_n\right)\exp(-q_n)\right. \\
+ & \mathcal{H}\frac{m_n[\tilde{\mathbf{v}}_n(\mathbf{r}-\mathbf{r}_n)]}{|\mathbf{r}-\mathbf{r}_n|^3}(\mathbf{r}-\mathbf{r}_n) \\
\times & \frac{9\left(1+q_n+q_n^2/3\right)\exp(-q_n) - \left(9+6\sqrt{3}q_n+4q_n^2\right)\exp\left(-2q_n/\sqrt{3}\right)}{q_n^2} \\
+ & \left.\mathcal{H}\frac{m_n\tilde{\mathbf{v}}_n}{|\mathbf{r}-\mathbf{r}_n|}\,\frac{\left(3+2\sqrt{3}q_n+4q_n^2\right)\exp\left(-2q_n/\sqrt{3}\right) - 3(1+q_n)\exp(-q_n)}{q_n^2}\right] .
\end{aligned}
\tag{3.16}
$$

The RHS of (3.12) is reduced to the Newtonian potential at small scales, i.e. when $q_n \ll 1$, and well describes the nonlinear dynamics relevant to structure growth at the sub-horizon level. Beyond the interaction range, however, the gravitational force is subject to exponential cutoff, which may be attributed to the relativistic effects inherent in the cosmic screening approach. Suppression of gravitational interactions at large-enough scales agrees with the cosmological principle as it implies the existence of an upper bound for the sizes of individual cosmic structures. Based on the Planck 2015 data [59], Eq. (3.5) of [1] yields $\lambda \approx 3.7\,\mathrm{Gpc}$ today.

3.2 The Effective Screening Length

3.2.1 The scheme of linear perturbation theory

Beyond the scale of nonlinearity, i.e. at large-enough scales, cosmological perturbations are often studied within the scope of the relativistic perturbation theory. A similar demonstration of screening is also present therein, provided that the scalar potential is only weakly dependent on time. This approach, i.e. cosmological screening from linear perturbation theory, was presented in [9], where the authors obtained a physical screening length al, interpreted in a similar way as its counterpart from the cosmic screening approach of discrete cosmology.

Linearized Einstein equations of the relativistic perturbation theory for the FRW spacetime and the flat ΛCDM model with solely nonrelativistic species have the form

$$
\triangle\Phi - 3\mathcal{H}\left(\Phi' + \mathcal{H}\Phi\right) = \frac{1}{2}\kappa a^2\delta\varepsilon\,, \tag{3.17}
$$

$$\Phi' + \mathcal{H}\Phi = -\frac{1}{2}\kappa a^2 \overline{\varepsilon}\nu\,, \tag{3.18}$$

$$\Phi'' + 3\mathcal{H}\Phi' + \left(2\mathcal{H}' + \mathcal{H}^2\right)\Phi = 0\,, \tag{3.19}$$

which coincides with (2.16) up to $\overline{p} = \delta\hat{p} = 0$ and $\hat{v} \to \nu$. The latter substitution merely follows from notation. Throughout the large-enough spatial regions relevant to this scheme, the energy density fluctuation $\delta\varepsilon$ always remains small in comparison to the background energy density $\overline{\varepsilon}$.

In [9], the function $\Phi(\eta, \mathbf{r})$ is decomposed as

$$\Phi = \frac{D_1}{a}\phi\,, \tag{3.20}$$

where $\phi = \phi(\mathbf{r})$ and $D_1(\eta)$ is the linear growth factor with the two solutions [50]

$$D_1^{(+)} \propto \frac{\mathcal{H}}{a}\int \frac{da}{\mathcal{H}^3}\,, \quad D_1^{(-)} \propto \frac{\mathcal{H}}{a}\,, \tag{3.21}$$

for the growing and decaying modes, respectively. The Helmholtz equation in this scheme, which again follows from the linearized Einstein equations, reads [9]

$$\triangle\Phi - 3\mathcal{H}\frac{D_1'}{D_1}\Phi = -\frac{1}{2}\kappa a^2 \delta\varepsilon\,, \tag{3.22}$$

with its own comoving screening length defined as

$$l \equiv \frac{1}{\sqrt{3\mathcal{H}^2 f}}\,, \quad f \equiv \frac{d\ln D_1}{d\ln a}\,. \tag{3.23}$$

It is important to note that the term $(D_1'/D_1)\Phi$ in Eq. (3.22) is related to the velocity potential $\nu(\eta, \mathbf{r})$ via

$$\frac{D_1'}{D_1}\Phi = -\frac{1}{2}\kappa a^2 \varepsilon\nu\,. \tag{3.24}$$

3.2.2 Combining the screening mechanisms of discrete cosmology and linear perturbation theory

The Helmholtz-type equation in (3.22) has a single source proportional to the energy density fluctuation. Meanwhile, its counterpart from discrete cosmology has one term proportional to the mass density fluctuation and one proportional to the function Ξ, which is associated with peculiar velocities. Looking back at (3.9) for comparison purposes, one realizes that the scalar potential contributes to the energy density perturbation through the relation

$$\delta\varepsilon = \frac{c^2}{a^3}\delta\rho + \frac{3\overline{\rho}c^2}{a^3}\Phi, \tag{3.25}$$

whereas the velocity potential, since it is no longer a source of the Helmholtz equation (3.22), is converted to the scalar perturbation itself as explicitly shown in (3.24).

Linear perturbation theory breaks down at sub-horizon distances where density fluctuations exceed the average value. Meanwhile, here the peculiar velocities and hence the Ξ term of discrete cosmology become insignificant and the Helmholtz equation (3.9) is safely reduced to the standard Poisson equation (given that, of course, the term $\propto \Phi$ on the LHS is also negligible). This is a key feature in accurately describing nonlinear dynamics governing small-scale cosmological processes. Based on this, i.e. the fact that peculiar motion is only relevant to large scales and that the screening ranges of both approaches are both much larger than the scale of nonlinearity (of the order of $10^1\,\mathrm{Mpc}$ today), the source term $\propto \Xi$ in (3.9) may be safely re-expressed via the velocity potential of the relativistic theory, as shown in [10], which eventually yields the novel Helmholtz equation

$$\triangle\Phi - \frac{a^2}{\lambda_{\text{eff}}^2}\Phi = \frac{\kappa c^2}{2a}\delta\rho\,, \tag{3.26}$$

where

$$\frac{1}{\lambda_{\text{eff}}^2} \equiv \frac{1}{\lambda^2} + \frac{1}{a^2 l^2} = \frac{3}{a\mathcal{H}}\left(\int \frac{da}{\mathcal{H}^3}\right)^{-1}\,. \tag{3.27}$$

Eq. (3.26) has a single velocity-free source proportional to the mass density fluctuation, which is analytically determined by the positions of gravitating bodies. Its exact solution follows as [10]

$$\Phi = \frac{1}{3}\left(\frac{\lambda_{\text{eff}}}{\lambda}\right)^2 - \frac{\kappa c^2}{8\pi a}\sum_n \frac{m_n}{|\mathbf{r}-\mathbf{r}_n|}\exp\left(-\frac{a|\mathbf{r}-\mathbf{r}_n|}{\lambda_{\text{eff}}}\right)\,. \tag{3.28}$$

The effective physical screening length λ_{eff} is calculated via the relation in (3.27), provided that one employs the growing mode of the linear growth factor $D_1^{(+)}$ in (3.21). Using recent Planck data [60], i.e. $H_0 = 67.4\,\mathrm{km\,s^{-1}Mpc^{-1}}$, $\Omega_{\mathrm{M}} = 0.315$, and $\Omega_\Lambda = 0.685$, for

$$H = H_0\sqrt{\Omega_M\left(\frac{a_0}{a}\right)^3 + \Omega_\Lambda}\,, \quad \Omega_M \equiv \frac{\kappa\overline{\rho}c^4}{3H_0^2 a_0^3}\,, \quad \Omega_\Lambda \equiv \frac{\Lambda c^2}{3H_0^2}\,, \tag{3.29}$$

the effective screening length today is found to be $2.57\,\mathrm{Gpc}$. As seen in Fig. (3.1), it agrees perfectly with the size of Hercules-Corona Borealis Great Wall (Her-CrB GW), the largest cosmic structure yet observed, with a reported size of 2 to $3\,\mathrm{Gpc}$ [61, 62].

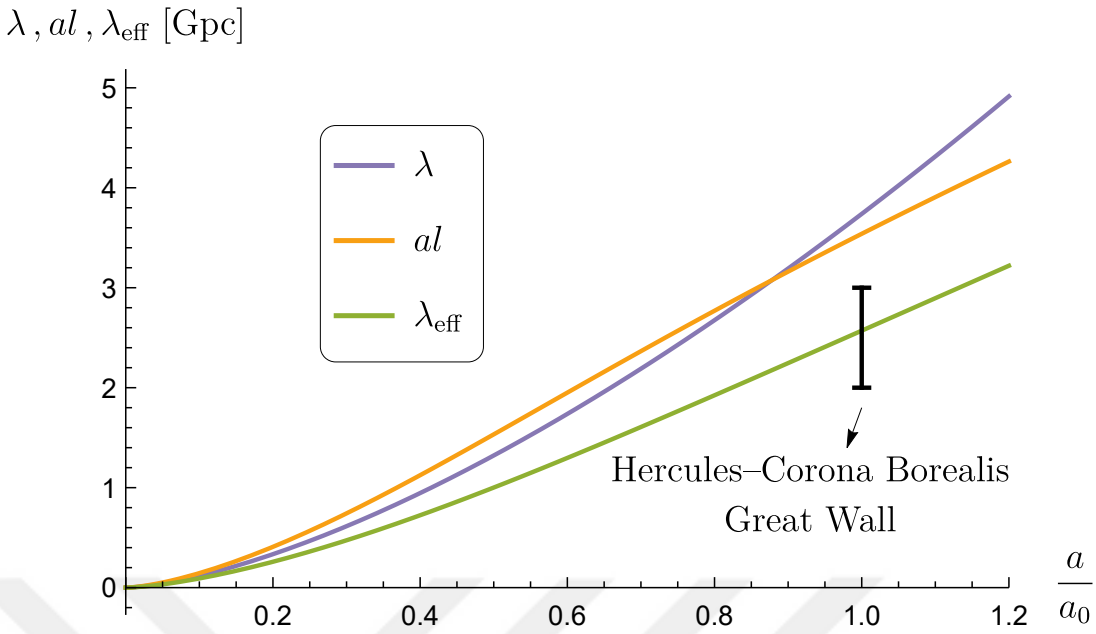

Figure 3.1 : The physical screening lengths of discrete cosmology, the relativistic perturbation theory, and that of the combined scheme of both approaches, i.e. λ, al, and λ_{eff}, respectively, plotted against the normalized scale factor a/a_0 [10].

3.2.3 Structure growth and the effective screening length

During the matter dominated epoch, i.e. setting $\Omega_\Lambda = 0$ in (3.29) so that $H \propto a^{-3/2}$, $\lambda_{\text{eff}} = \sqrt{2/15}(c/H)$ appears to be smaller than both interaction ranges from combined approaches: $\lambda_{\text{eff}} < \lambda = \sqrt{2}/3(c/H) < al = 1/\sqrt{3}(c/H)$. Meanwhile, according to Eqs. (35)-(37) of [10], density fluctuations in Fourier space grow proportional to $k^2\phi_k\,[a + 5\kappa\bar{\rho}c^2/(2k^2)]$. This relation specifies the comoving scale below which, in the matter era, $\delta\rho_k$ grows significantly: $k^{-1} = \sqrt{2a/\left(5\kappa\bar{\rho}c^2\right)}$. As $ak^{-1} = \lambda_{\text{eff}}$, one may deduce that the effective screening length, which indicates the Yukawa range of the combined approach, sets an upper limit on the sizes of domains in which structure growth takes place.

3.3 On the Importance of Peculiar Velocities in the Screening Approach

The equation of motion of the $k-$th particle in the system (3.16) shows that the force per unit mass, induced by the n-th ($n \neq k$) particle, consists solely of terms with exponentially decaying functions. This expression well confirms that force decreases exponentially with distance from the gravitating source.

Further elaborating on this formula, one may consider the possibility of neglecting the somewhat complex velocity-dependent terms here. Indeed, in terms of the current values of the Hubble parameter, the screening length and typical peculiar velocities, that are $H_0 \approx 70\,\mathrm{km\,s^{-1}Mpc^{-1}}$, $\lambda_0 \approx 3.7\,\mathrm{Gpc}$ and $(av_n)_0 \sim 250 - 500\,\mathrm{km\,s^{-1}}$, where $av_n = c\tilde{v}_n$, the ratio of the overall velocity-dependent part to the single term without $\tilde{\mathbf{v}}_n$, which is of the order of $3H\lambda av_n/c^2$ [10], is $\sim 2 - 4 \times 10^{-3}$. Moreover, the ratio of the velocity-dependent last term in the scalar perturbation (3.12) to the term without $\tilde{\mathbf{v}}_n$ always remains small within the typically used cosmological simulation boxes: it is about $1 - 2\%$ for $q_n \leq 3$, which corresponds to physical distances less than or equal to $11\,\mathrm{Gpc}$ [1, 10, 45]. Consequently, one might come to the conclusion that it is actually possible to lose the velocity dependence in Eqs. (3.12) (and (3.16)). It amounts to limiting oneself to the velocity-free piece of the scalar perturbation Φ, obtained by solving the Helmholtz equation (3.9), now without the source containing Ξ.

Nevertheless such an estimation is misleading. Neglecting the velocity dependent term in Φ results in a faulty description of structure growth at large scales (see Sect. (3) of [10] for a detailed discussion). Indeed, the gravitational field generated by a solitary delta-shaped mass and that of some continuous mass distribution cannot be handled identically. Modelling the finite-size mass overdensity as some ball of comoving radius r_b, and uniform mass density ρ_b, the velocity-free Helmholtz equation gives the first piece of the potential expression labeled $\tilde{\Phi}_b$, sourced solely by the mass overdensity [10]:

$$\tilde{\Phi}_b = -\frac{\kappa c^2 \lambda^3}{2a^4}\frac{\rho_b - \overline{\rho}}{r}\left[\frac{ar_b}{\lambda}\cosh\left(\frac{ar_b}{\lambda}\right) - \sinh\left(\frac{ar_b}{\lambda}\right)\right]\exp\left(-\frac{ar}{\lambda}\right) . \tag{3.30}$$

Only the regions outside the ball are meaningful, so the expression holds only for distances greater than the radius of the ball - for $r > r_b$. Considering the motion of the ball to be along the direction of the position vector r, one obtains the second piece of the scalar perturbation Φ_{vb} as [10]

$$\begin{aligned}\Phi_{vb} &= -\frac{3\kappa c^2 \mathcal{H}\lambda^5}{2a^6}\frac{\rho_b \tilde{v}_b}{r^2} \\ \times\ &\left\{-\frac{1}{3}\left(\frac{ar_b}{\lambda}\right)^3 + \left(1 + \frac{ar}{\lambda}\right)\left[\frac{ar_b}{\lambda}\cosh\left(\frac{ar_b}{\lambda}\right) - \sinh\left(\frac{ar_b}{\lambda}\right)\right]\exp\left(-\frac{ar}{\lambda}\right)\right\} ,\end{aligned} \tag{3.31}$$

sourced instead by the $\Xi-$term and again, valid for distances outside the mass distribution only. The ratio of Φ_{vb} to $\tilde{\Phi}_b$ is proportional to the product

$(3\mathcal{H}\lambda\tilde{v}_b/a)\,(\rho_b/(\rho_b-\overline{\rho}))$. The previously calculated "small" prefactor, of the order of 10^{-3}, is compensated here by the ratio $(\rho_b/(\rho_b-\overline{\rho}))$, which increases with the increasing size of the ball as ρ_b approaches $\overline{\rho}$ for large r_b. Thereby, it appears that ignoring peculiar motion leads to an incorrect formulation of gravitational interactions at larger distances.

3.4 Peculiar Velocity Contributions in Curved Space

In [6], the original scheme of cosmic screening [1] was revisited to study the behaviour of the gravitational potential in curved space, i.e. in open and closed universes. Peculiar velocities of discrete sources were entirely disregarded in the formulation. It was revealed that in an open universe, the potential would undergo an exponential decay with increasing distance from the source, as in flat space, though the $1/r$ prefactor in the zero curvature case would be replaced by $1/\sinh l$, l indicating the geodesic distance from the location of the source. In a closed universe, the shape of the gravitational potential would depend on the scale factor to take on different forms with growing a - but no exponential decay in any epoch.

The Planck 2018 combined cosmic microwave background (CMB) and baryon acoustic oscillations measurements strongly favour a flat universe [60]. However, the combined Planck temperature and polarization power spectra data reports a mildly closed hypersurface with $\Omega_K = -0.044^{+0.018}_{-0.015}$, where Ω_K indicates the spatial curvature parameter in the homogeneous and isotropic universe. Given the ambiguity in observational results regarding the curvature parameter, it appears to be a nontrivial task to revisit the effective screening length, that readily incorporates the effect of peculiar velocities, in curved space in search of a broader picture of gravitational interactions in the cosmological setting.

3.4.1 The background for constant curvature spaces

The background FRW metric has the form

$$ds^2 = a^2(\eta)\left[d\eta^2 - \gamma_{\alpha\beta}\,dx^\alpha dx^\beta\right] = a^2(\eta)\left[d\eta^2 - d\chi^2 - \Sigma^2(\chi)\,d\Omega^2\right], \qquad (3.32)$$

for the most general constant-curvature space, for which the function $\Sigma(\chi)$ is defined as

$$\Sigma(\chi) = \begin{cases} \sin\chi, & \chi \in [0,\pi] \text{ for } \mathcal{K}=+1 \\ \chi, & \chi \in [0,+\infty) \text{ for } \mathcal{K}=0 \\ \sinh\chi, & \chi \in [0,+\infty) \text{ for } \mathcal{K}=-1 \end{cases} \tag{3.33}$$

and $d\Omega^2 \equiv d\theta^2 + \sin^2\theta d\phi^2$. Open, flat and closed universes are represented by $\mathcal{K} = -1, 0, +1$, respectively.

From this metric, one obtains the Friedmann equation

$$\frac{3(\mathcal{H}^2+\mathcal{K})}{a^2} = \kappa\bar{\varepsilon} + \Lambda\,, \tag{3.34}$$

or, in terms of the dimensionless cosmological parameters defined in (3.29),

$$H = H_0\sqrt{\Omega_M\left(\frac{a_0}{a}\right)^3 + (1-\Omega_M-\Omega_\Lambda)\left(\frac{a_0}{a}\right)^2 + \Omega_\Lambda} \tag{3.35}$$

for a universe that consists of pressureless nonrelativistic matter in the presence of the cosmological constant.

3.4.2 The scalar potential

In curved space, the expression for the comoving mass density of discrete inhomogeneities is modified as

$$\rho = \frac{1}{\sqrt{\gamma}}\sum_i m_i\,\delta(\mathbf{r}-\mathbf{r}_i)\;, \quad \gamma \equiv \det[\gamma_{\alpha\beta}], \tag{3.36}$$

and in the presence of these gravitating bodies, the perturbed spacetime is described by the metric

$$ds^2 = a^2\left[(1+2\Phi)d\eta^2 - (1-2\Phi)\gamma_{\alpha\beta}\,dx^\alpha dx^\beta\right], \tag{3.37}$$

when the vector and tensor perturbations are disregarded. Einstein equations of the linear perturbation theory follow as [49]

$$\triangle\Phi - 3\mathcal{H}\left(\Phi' + \mathcal{H}\Phi\right) + 3\mathcal{K}\Phi = \frac{1}{2}\kappa a^2\delta\varepsilon\,, \tag{3.38}$$

$$\Phi' + \mathcal{H}\Phi = -\frac{1}{2}\kappa a^2\bar{\varepsilon}v\,, \tag{3.39}$$

$$\Phi'' + 3\mathcal{H}\Phi' + \left(2\mathcal{H}' + \mathcal{H}^2 - \mathcal{K}\right)\Phi = 0\,, \tag{3.40}$$

where the Laplace operator $\triangle = \left(1/\sqrt{\gamma}\right)\partial_\alpha\left(\sqrt{\gamma}\,\gamma^{\alpha\beta}\partial_\beta\right)$.

Once again, using the ansatz given by (3.20) together with the relation $\delta\varepsilon = c^2\delta\rho/a^3 + 3\overline{\rho}c^2\Phi/a^3$, Eq. (3.38) yields [11]

$$\triangle\Phi - 3\left(\mathcal{H}\frac{D_1'}{D_1} + \frac{\kappa\overline{\rho}c^2}{2a} - \mathcal{K}\right)\Phi = \frac{\kappa c^2}{2a}\delta\rho\,, \tag{3.41}$$

or,

$$\triangle\Phi - \frac{a^2}{\lambda_{\rm eff}^2}\Phi = \frac{\kappa c^2}{2a}\delta\rho\,. \tag{3.42}$$

The $1/\lambda_{\rm eff}^2$ term is decomposed in the same way as in (3.27), however, now the $1/l^2$ term is re-defined due to the additional contribution of nonzero spatial curvature:

$$\frac{1}{l^2} \equiv 3\mathcal{H}\frac{D_1'}{D_1} - 3\mathcal{K} = 3\mathcal{H}^2\frac{d\ln D_1}{d\ln a} - 3\mathcal{K}\,. \tag{3.43}$$

The first term on the RHS is associated with peculiar velocities of gravitating sources and in [10], it was shown that when peculiar velocities were included in the formulation, the cutoff range of Yukawa interactions decreased from $3.74\,{\rm Gpc}$ to $2.57\,{\rm Gpc}$. It is seen clearly here that they have a similar impact in curved spaces as well. However, extra curvature term itself does not significantly affect $\lambda_{\rm eff}$. In fact, substituting the growing solution (3.21) in (3.43), and employing the Friedmann equation (3.34), one finds that

$$\begin{aligned}\frac{1}{\lambda_{\rm eff}^2} &= \frac{3\kappa\overline{\rho}c^2}{2a^3} + \frac{3\mathcal{H}}{a^2}\left[\frac{a}{\mathcal{H}^2}\left(\int\frac{da}{\mathcal{H}^3}\right)^{-1} + \left(a\frac{d\mathcal{H}}{da} - \mathcal{H} - \frac{\mathcal{K}}{\mathcal{H}}\right)\right] \\ &= \frac{3}{Ha^2c^2}\left(\int\frac{da}{a^3H^3}\right)^{-1}\,,\end{aligned} \tag{3.44}$$

which is identical in form to (3.27) obtained previously for $\mathcal{K} = 0$.

In terms of a new parameter $\nu \equiv a^2/\lambda_{\rm eff}^2$ introduced in (25) of [11], solutions of (3.42) were also obtained for the $\mathcal{K} = -1, +1$ cases:

$$\Phi = \frac{4\pi G_N}{c^4}\overline{\varepsilon}\lambda_{\rm eff}^2 - \frac{G_N}{c^2a}\sum_i\frac{m_i}{\sinh\,l_i}\,\exp\left(-\sqrt{\nu+1}l_i\right)\,, \quad \mathcal{K} = -1\,, \tag{3.45}$$

and

$$\Phi = \frac{4\pi G_N}{c^4}\overline{\varepsilon}\lambda_{\rm eff}^2 - \frac{G_N}{c^2a}\sum_i m_i\frac{\sinh\left[\sqrt{\nu-1}(\pi - l_i)\right]}{\sinh\left(\sqrt{\nu-1}\pi\right)\sin l_i}\,, \quad \mathcal{K} = +1\,, \tag{3.46}$$

where l_i specifies the geodesic distance between the test point and the $i-$th particle with mass m_i .

In [6], for $\mathcal{K} = +1$, three different expressions were obtained for the gravitational potential for growing a, which brought along the requirement that these solutions be

connected smoothly to one another. In [11], taking into account peculiar velocities, and thereby, adopting a more complete approach, it has been shown that there exists a single expression for the potential Φ in a closed universe for all the values of a relevant to structure growth.

4. GRAVITATIONAL POTENTIAL AND FORCE IN PERIODIC BOUNDARIES

The theory of GR does not specify whether the space is flat, open or closed. Neither does it favour a simply connected universe over a multiply connected one. Indeed, certain features of CMB temperature patterns are studied broadly in search of topologies other than that of the infinite simply-connected universe with flat spatial geometry [63, 64, 65, 66, 67, 68], as is the predicted shape of the universe in concordance cosmology. In a multiply connected universe, negative and zero curvature spaces could have finite volume. The cubic toroidal topology sets an interesting example for this for the zero-curvature case, given that it would be possible to relate the quadrupole moment suppression at large angular scale CMB observations to the existence of sufficiently compact spaces with dimensions of the same order of magnitude [69, 70].

On the other hand, fully periodic boundaries are essential to the N-body codes to properly simulate the infinite universe of the ΛCDM model. Conventionally, these codes make use of cubic domains replicated along three dimensions while solving for the gravitational force [15, 16, 17, 18].

Based on such motivations, the Helmholtz equation in (3.26) was revisited in [12] and it was solved for the periodic potential for the cubic toroidal topology. The resulting alternative expressions (together with the expressions for the gravitational force) were then studied in view of numerical efficiency.

4.1 Helmholtz Equation in the Fully Periodic Cubic Domain

Re-expressing the Helmholtz equation (3.26) in terms of the shifted potential $\hat{\Phi}$, defined as [12]

$$\widehat{\Phi} \equiv \Phi - \lambda_{\text{eff}}^2 \frac{\kappa c^2}{2a^3} \bar{\rho}\,, \tag{4.1}$$

one obtains

$$\Delta\widehat{\Phi} - \frac{a^2}{\lambda_{\text{eff}}^2}\widehat{\Phi} = \frac{\kappa c^2}{2a}\rho\,. \tag{4.2}$$

Now, the source on the RHS is the mass density instead of the mass density fluctuation $\delta\rho$, and thereby, from the superposition principle, the solution for this equation for a single particle at $x = y = z = 0$ may be generalized to express the potential due to a collection of randomly positioned point sources as well.

For the cubic torus topology $T \times T \times T$, and placing a single delta-shaped mass at the origin, one way to express the solution of (4.2) is to add the Yukawa potentials sourced by the original mass and its infinitely many periodic images, that is [12]

$$\begin{aligned}
&\tilde{\Phi}_{\text{exp}} \equiv \left(-\frac{G_N m}{c^2 a l}\right)^{-1} \widehat{\Phi}_{\text{exp}} \\
&= \sum_{k_1=-\infty}^{+\infty} \sum_{k_2=-\infty}^{+\infty} \sum_{k_3=-\infty}^{+\infty} \frac{1}{\sqrt{(\tilde{x}-k_1)^2+(\tilde{y}-k_2)^2+(\tilde{z}-k_3)^2}} \\
&\times \exp\left(-\frac{\sqrt{(\tilde{x}-k_1)^2+(\tilde{y}-k_2)^2+(\tilde{z}-k_3)^2}}{\tilde{\lambda}_{\text{eff}}}\right).
\end{aligned} \tag{4.3}$$

Alternatively, Ewald summations may be employed so that the Yukawa potentials in periodic boundaries can be formulated as two distinct series in real and Fourier spaces with good convergence properties [12]

$$\begin{aligned}
&\tilde{\Phi}_{\text{mix}} \equiv \left(-\frac{G_N m}{c^2 a l}\right)^{-1} \widehat{\Phi}_{\text{mix}} \\
&= \sum_{k_1=-\infty}^{+\infty} \sum_{k_2=-\infty}^{+\infty} \sum_{k_3=-\infty}^{+\infty} \left\{ \frac{D\left(\sqrt{(\tilde{x}-k_1)^2+(\tilde{y}-k_2)^2+(\tilde{z}-k_3)^2}; \alpha; \tilde{\lambda}_{\text{eff}}\right)}{2\sqrt{(\tilde{x}-k_1)^2+(\tilde{y}-k_2)^2+(\tilde{z}-k_3)^2}} \right. \\
&+ \left. 4\pi \cos\left[2\pi\left(k_1\tilde{x}+k_2\tilde{y}+k_3\tilde{z}\right)\right] \frac{\exp\left[-\left(4\pi^2 k^2 + \tilde{\lambda}_{\text{eff}}^{-2}\right)/\left(4\alpha^2\right)\right]}{4\pi^2 k^2 + \tilde{\lambda}_{\text{eff}}^{-2}} \right\},
\end{aligned} \tag{4.4}$$

where $k^2 \equiv k_1^2 + k_2^2 + k_3^2$, and

$$\begin{aligned}
&D\left(\sqrt{(\tilde{x}-k_1)^2+(\tilde{y}-k_2)^2+(\tilde{z}-k_3)^2}; \alpha; \tilde{\lambda}_{\text{eff}}\right) \\
&\equiv \exp\left(\frac{\sqrt{(\tilde{x}-k_1)^2+(\tilde{y}-k_2)^2+(\tilde{z}-k_3)^2}}{\tilde{\lambda}_{\text{eff}}}\right) \\
&\times \operatorname{erfc}\left(\alpha\sqrt{(\tilde{x}-k_1)^2+(\tilde{y}-k_2)^2+(\tilde{z}-k_3)^2} + \frac{1}{2\alpha\tilde{\lambda}_{\text{eff}}}\right) \\
&+ \exp\left(-\frac{\sqrt{(\tilde{x}-k_1)^2+(\tilde{y}-k_2)^2+(\tilde{z}-k_3)^2}}{\tilde{\lambda}_{\text{eff}}}\right) \\
&\times \operatorname{erfc}\left(\alpha\sqrt{(\tilde{x}-k_1)^2+(\tilde{y}-k_2)^2+(\tilde{z}-k_3)^2} - \frac{1}{2\alpha\tilde{\lambda}_{\text{eff}}}\right).
\end{aligned} \tag{4.5}$$

The rescaled quantities with tilde are defined via $\tilde{x}l = x$, $\tilde{y}l = y$, $\tilde{z}l = z$ and $al\tilde{\lambda}_{\text{eff}} = \lambda_{\text{eff}}$, where a and l are the scale factor and the period of the cubic torus,

respectively. In (4.5), erfc denotes the complementary error function [71] and the α-parameter of Ewald formulation, when assigned an optimal value, allows for rapid convergence and good precision at low computational cost. For the range of $\tilde{\lambda}_{\text{eff}}$ studied in [12], this optimal value was found to be 2.

N-body simulations based on the Newtonian approximation usually resort to this formulation [72, 73] because using Ewald sums, the force series with bad convergence becomes manageable in numerical calculations. Ewald sums are also encountered in studies investigating electrostatic interactions characterized by the Yukawa law, and within such context, the fully periodic Yukawa-Ewald potential was derived previously in [74].

4.1.1 Comparing the two formulas

Owing to periodicity, both expressions (4.3) and (4.4) include infinite series. In order to numerically determine $\tilde{\Phi}$ at a given point to good accuracy and with minimum computational effort, it is important to know which of these formulas require the least number n of summands in the series. In [12], such a comparison was performed based on the numbers n_{exp} and n_{mix}, and it was revealed that for $\tilde{\lambda}_{\text{eff}} \ll 1$, both the Yukawa (4.3) and Yukawa-Ewald (4.4) formulas required the same number of image contributions to reach the targeted accuracy at points $(\tilde{x}, \tilde{y}, \tilde{z})$ of interest. However, given the much simpler form of (4.3), it was concluded that this formula would be more preferable for computational purposes. Meanwhile, when $\tilde{\lambda}_{\text{eff}} \geq 1$, it was the Yukawa-Ewald potential (4.4) that provided the best results, especially after $\tilde{\lambda}_{\text{eff}}$ exceeded the box size.

It is worth highlighting that the potential expressions presented above are both sensitive to $\tilde{\lambda}_{\text{eff}}$. As previously indicated, this quantity is defined as $\tilde{\lambda}_{\text{eff}} = \lambda_{\text{eff}}/(al)$. Currently, $\lambda_{\text{eff}} \sim 2.6\,\mathrm{Gpc}$ according to the concordance model [10], and the dimensions al for the studied T^3 geometry are bounded from below by Planck 2015 results by $\sim 27\,\mathrm{Gpc}$ [75], which brings along the constraint $\tilde{\lambda}_{\text{eff}} \ll 1$ for a physically relevant analysis. However, most N-body simulations are run in cells with dimensions smaller than $1\,\mathrm{Gpc}$, therefore, for completeness, the cases where $\tilde{\lambda}_{\text{eff}} \geq 1$ have also been considered in the work [12].

Performing a similar comparison with respect to numbers n for the $x-$components of the gravitational forces $\partial_{\tilde{x}}\tilde{\Phi}_{\cos}$, $\partial_{\tilde{x}}\tilde{\Phi}_{\exp}$ and $\partial_{\tilde{x}}\tilde{\Phi}_{\mathrm{mix}}$, same ranking of performances was observed as that of gravitational potentials [12]. The Yukawa force was a better choice in view of its plainness because the numbers $n_{\exp}$ and n_{mix} remained the same up to $\tilde{\lambda}_{\mathrm{eff}} = 0.1$. The Yukawa-Ewald formula has a rather complex structure and thus, in general, more computation time is required to numerically calculate the force in this case.

4.1.2 Remarks on the relation between periodic formulation and the Yukawa range

In the above formulation, periodicity manifests itself in the contribution of replicated images of the gravitating source. It is quantified by the numbers n calculated for the potential and force formulas. In [12], it was pointed out that particularly for the Yukawa-type solutions, the number $n_{\exp}$ decreased for smaller values of the ratio $\lambda_{\mathrm{eff}}/(al)$. In other words, using boxes that are large-enough compared to the screening length, impacts of periodicity will show less in the potential (and thereby, force) calculations.

Assuming an infinite universe, periodic boundaries turn out to be merely artificial adjustments in N-body codes. From that perspective, employing the Yukawa law in the equations of motion solved in these codes as well as using a large-enough simulation box, one may better describe the interactions in the *actual* physical setting, i.e. the infinite space which also agrees with the ΛCDM model.

4.2 Comparison of Yukawa and Newtonian Laws of Gravitation in Cubic Domain with Periodic Boundaries

With the intention of introducing Yukawa gravity in future simulations of structure formation as an alternative to the Newtonian approximation, the distances at which the Yukawa and Newtonian gravitational forces began to diverge from one another were investigated lately in the work [76]. Fully periodic boundaries in a cubic domain were assumed to mimic the typical structure of most of the available simulation codes.

For a single particle in a cubic box with three-dimensional periodicity, $x-$component of the rescaled Yukawa-Ewald force $\tilde{F}_{\rm YE}$, derived from (4.4), reads

$$\begin{aligned}
\tilde{F}_{\rm YE} \equiv \frac{\partial\tilde{\Phi}_{\rm YE}}{\partial\tilde{x}} = -\frac{1}{2}\sum_{k_1=-\infty}^{+\infty}\sum_{k_2=-\infty}^{+\infty}\sum_{k_3=-\infty}^{+\infty}\Bigg[&(\tilde{x}-k_1)\\
\times\ & \frac{D\left(\sqrt{(\tilde{x}-k_1)^2+(\tilde{y}-k_2)^2+(\tilde{z}-k_3)^2};\alpha;\tilde{\lambda}_{\rm eff}\right)}{\left[(\tilde{x}-k_1)^2+(\tilde{y}-k_2)^2+(\tilde{z}-k_3)^2\right]^{3/2}}\\
+\ & \frac{\tilde{x}-k_1}{(\tilde{x}-k_1)^2+(\tilde{y}-k_2)^2+(\tilde{z}-k_3)^2}\\
\times\ & C_-\exp\left(-\frac{\sqrt{(\tilde{x}-k_1)^2+(\tilde{y}-k_2)^2+(\tilde{z}-k_3)^2}}{\tilde{\lambda}_{\rm eff}}\right)\\
+\ & \frac{\tilde{x}-k_1}{(\tilde{x}-k_1)^2+(\tilde{y}-k_2)^2+(\tilde{z}-k_3)^2}\\
\times\ & C_+\exp\left(\frac{\sqrt{(\tilde{x}-k_1)^2+(\tilde{y}-k_2)^2+(\tilde{z}-k_3)^2}}{\tilde{\lambda}_{\rm eff}}\right)\\
+\ & 16\pi^2k_1\sin\left[2\pi\left(k_1\tilde{x}+k_2\tilde{y}+k_3\tilde{z}\right)\right]\frac{\exp\left[-\left(4\pi^2k^2+\tilde{\lambda}_{\rm eff}^{-2}\right)/\left(4\alpha^2\right)\right]}{4\pi^2k^2+\tilde{\lambda}_{\rm eff}^{-2}}\Bigg]\,,
\end{aligned}\tag{4.6}$$

where,

$$\begin{aligned}
C_\mp = C_\mp\left(\sqrt{(\tilde{x}-k_1)^2+(\tilde{y}-k_2)^2+(\tilde{z}-k_3)^2};\alpha;\tilde{\lambda}_{\rm eff}\right)\\
\equiv\ \frac{2\alpha}{\sqrt{\pi}}\exp\left[-\left(\alpha\sqrt{(\tilde{x}-k_1)^2+(\tilde{y}-k_2)^2+(\tilde{z}-k_3)^2}\ \mp\ \frac{1}{2\alpha\tilde{\lambda}_{\rm eff}}\right)^2\right]\\
\pm\ \frac{1}{\tilde{\lambda}_{\rm eff}}\,{\rm erfc}\left(\alpha\sqrt{(\tilde{x}-k_1)^2+(\tilde{y}-k_2)^2+(\tilde{z}-k_3)^2}\mp\frac{1}{2\alpha\tilde{\lambda}_{\rm eff}}\right)\,.
\end{aligned}\tag{4.7}$$

On the other hand, its Newtonian counterpart which is already used in N-body codes, has the form [72, 73]

$$\begin{aligned}
\tilde{F}_{\rm NE} \equiv \frac{\partial\tilde{\Phi}_{\rm NE}}{\partial\tilde{x}} =\\
-\sum_{k_1=-\infty}^{+\infty}\sum_{k_2=-\infty}^{+\infty}\sum_{k_3=-\infty}^{+\infty}\Bigg[&(\tilde{x}-k_1)\ \frac{{\rm erfc}\left(\alpha\sqrt{(\tilde{x}-k_1)^2+(\tilde{y}-k_2)^2+(\tilde{z}-k_3)^2}\right)}{\left[(\tilde{x}-k_1)^2+(\tilde{y}-k_2)^2+(\tilde{z}-k_3)^2\right]^{3/2}}\\
+\ & \frac{2\alpha}{\sqrt{\pi}}\frac{\tilde{x}-k_1}{(\tilde{x}-k_1)^2+(\tilde{y}-k_2)^2+(\tilde{z}-k_3)^2}\\
\times\ & \exp\left[-\alpha^2\left((\tilde{x}-k_1)^2+(\tilde{y}-k_2)^2+(\tilde{z}-k_3)^2\right)\right]\Bigg]\\
-\ & 2\sum_{q_1=-\infty}^{+\infty}\sum_{\substack{q_2=-\infty\\ \mathbf{q}\neq 0}}^{+\infty}\sum_{q_3=-\infty}^{+\infty}q_1\sin\left[2\pi\left(q_1\tilde{x}+q_2\tilde{y}+q_3\tilde{z}\right)\right]\frac{\exp\left(-\pi^2q^2/\alpha^2\right)}{q^2}\,,\\
q^2 \equiv q_1^2+q_2^2+q_3^2\,.
\end{aligned}\tag{4.8}$$

For free boundaries, the two forces are

$$\tilde{F}_{\rm Y} \equiv \frac{\partial \tilde{\Phi}_{\rm Y}}{\partial \tilde{x}} = -\left[\frac{\tilde{x}}{(\tilde{x}^2+\tilde{y}^2+\tilde{z}^2)^{3/2}} + \frac{\tilde{x}/\tilde{\lambda}_{\rm eff}}{\tilde{x}^2+\tilde{y}^2+\tilde{z}^2}\right] \exp\left(-\frac{\sqrt{\tilde{x}^2+\tilde{y}^2+\tilde{z}^2}}{\tilde{\lambda}_{\rm eff}}\right), \tag{4.9}$$

$$\tilde{F}_{\rm N} \equiv \frac{\partial \tilde{\Phi}_{\rm N}}{\partial \tilde{x}} = -\frac{\tilde{x}}{(\tilde{x}^2+\tilde{y}^2+\tilde{z}^2)^{3/2}}, \tag{4.10}$$

again, for the single mass located at the origin. The rescaled quantities with tilde are defined in the same way as those introduced in Sect. (4.1). Here also, for simplicity, calculations are restricted to the the $x-$components of the force expressions only.

In Fig. (4.1), plain and periodic Yukawa and Newtonian force curves are plotted simultaneously against the distance $\tilde{x}$ from the source for four different values of the rescaled screening length. In Figs. (5.1a) and (5.1b), where $\tilde{\lambda}_{\rm eff} \ll 1$, two sets of curves that belong to different laws remain well separated from one another, excluding the region that marks the immediate neighbourhood of the source and near $\tilde{x} = 0.5$, where both periodic forces tend to zero. Periodic forces do not differ much from the free-boundary forces of the same law throughout. Meanwhile, in Figs. (5.1c) and (5.1d), i.e. for larger $\tilde{\lambda}_{\rm eff}$, the Yukawa-Ewald and Newton-Ewald curves coincide (or, differ very slightly), and so do the non-periodic Yukawa and Newtonian curves, and now it is the periodic and plain forces sets that are separated.

For small values of the effective screening length, which is the parameter specifying the range of the exponentially decaying Yukawa force, behaviours of Yukawa and Newtonian forces begin to differ at small scales (of course, with respect to the box size) as expected. In this case, periodicity does not have a significant impact on the behaviour of the Yukawa force as it decays very fast to join the Yukawa-Ewald curve, which goes to zero moving towards the edge of the box ($\tilde{x} = 0.5$), irrespective of how large/small $\tilde{\lambda}_{\rm eff}$ is. However, when $\tilde{\lambda}_{\rm eff}$ is comparable to the box size, in the free-boundary case, the larger screening length prevents rapid decay within the range of interest and periodicity requires otherwise. Consequently, the plain and and periodic forces differ from one another. For the same reason, Yukawa and Newtonian curves behave similarly even about $\tilde{x} = 0.5$, i.e. the edge of the box, which is a small enough distance compared to the cutoff scale now.

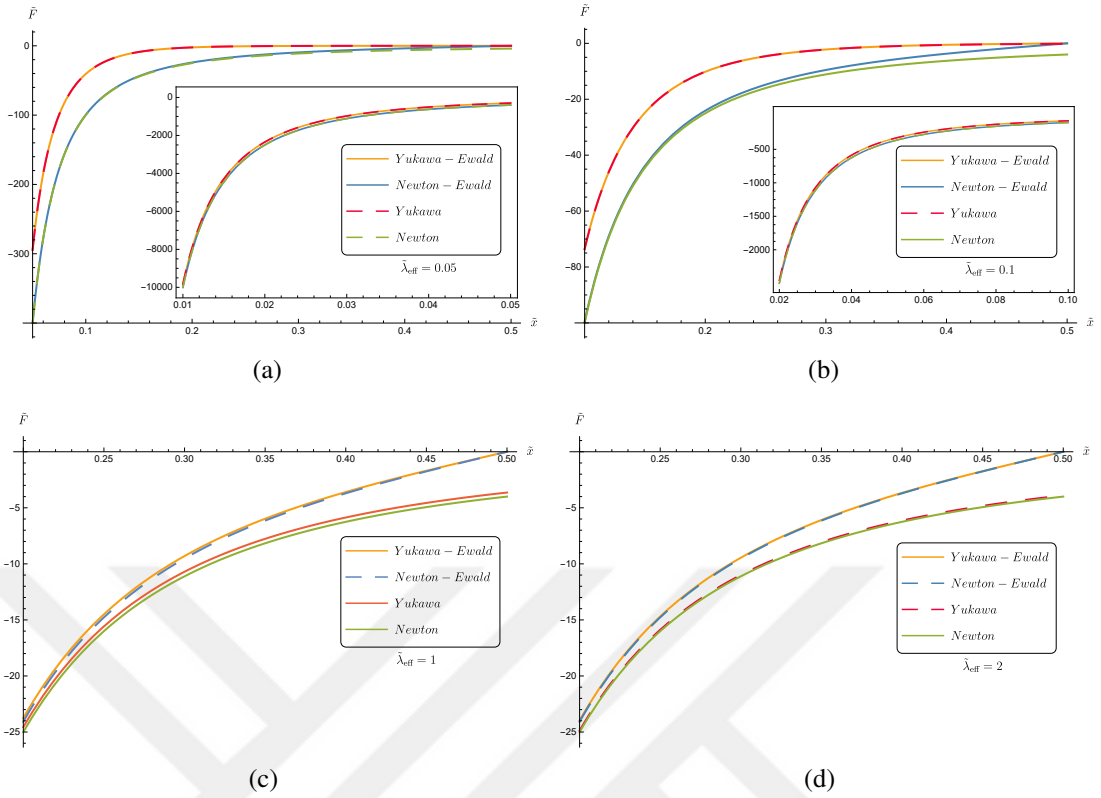

Figure 4.1 : x-components of the plain and periodic gravitational forces $\tilde{F} \equiv \partial\tilde{\Phi}/\partial\tilde{x}$ on the $y = z = 0$ line for (a) $\tilde{\lambda}_{\rm eff} = 0.1$, (b) $\tilde{\lambda}_{\rm eff} = 1$, (c) $\tilde{\lambda}_{\rm eff} = 1$ and (d) $\tilde{\lambda}_{\rm eff} = 2$ [76].

Introducing the relative difference $|(\tilde{F}_{\rm YE} - \tilde{F}_{\rm NE})/\tilde{F}_{\rm YE}|$, it was shown in [76] that, for instance, when $\tilde{\lambda}_{\rm eff}$ is set to 0.1, the 1% difference is encountered slightly past $\tilde{x} = 0.01$ (as demonstrated in Fig. (5.2a)) and for smaller values of the screening length, it appears even closer to the gravitating body. In a box with a physical size of $a_0 l = 1.3\,{\rm Gpc}$ today (at $z = 0$), $\tilde{\lambda}_{\rm eff}$ should be set to 2 according to $\lambda_{\rm eff} = (a/a_0)(a_0 l)\tilde{\lambda}_{\rm eff}$, given that $\lambda_{\rm eff} \sim 2.6\,{\rm Gpc}$ today [10]. In such configuration, the 1% difference takes place at $x \sim 530\,{\rm Mpc}$ and going down to 0.001%, the distance gets as small as $x \sim 12\,{\rm Mpc}$, which corresponds to the point $\tilde{x} = 0.00898$ on the $y-$axis in Fig (5.2b). Earlier in [15], the error associated with the plain Newtonian and Newton-Ewald forces was studied to reveal the impact of periodicity involved in cosmological simulations. It was shown that 0.001% error appeared at about $x = 0.01l$. In [76], with respect to Yukawa and Newtonian laws of gravity in periodic boundaries, the same percent difference was found at a distance less than 1% of the box size ($12\,{\rm Mpc}$ away from the source in a $1.3\,{\rm Gpc}$ box), highlighting the somewhat stronger discrepancy between the two forces. Moreover, the difference grew stronger looking back into the matter-dominated era: at $z = 119$, which is the leftmost point on the

$x-$axis of Fig. (5.2b), at $\tilde{\lambda}_{\text{eff}} = 0.2$, location of the 1% difference is found to be $\tilde{x} = 0.000896$, i.e. $\sim 9.71 \times 10^{-3}\text{Mpc}$ in a $\sim 10.8\,\text{Mpc}$ simulation box.

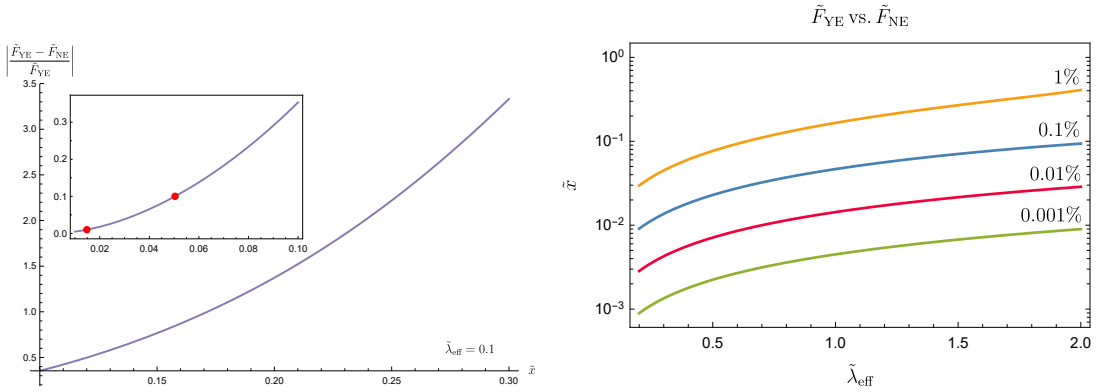

(a) (b)

Figure 4.2 : (a) Relative difference calculated with respect to the x-components of the Yukawa-Ewald and Newton-Ewald forces for $\tilde{\lambda}_{\text{eff}} = 0.1$ on the $\tilde{y} = \tilde{z} = 0$ line. From left to right, the two dots mark the positions of the 1% $(\tilde{x} = 0.0148)$ and 10% $(\tilde{x} = 0.0504)$ differences, respectively. (b) Locations of four percent differences in the box plotted as functions of $\tilde{\lambda}_{\text{eff}}$ for the $\tilde{F}_{\text{YE}}$ vs. $\tilde{F}_{\text{NE}}$ forces on the $\tilde{y} = \tilde{z} = 0$ line. Moving downwards from the 1% difference, the curves lie between the points 0.0297–0.408 (1%), 0.00909–0.0938 (0.1%), 0.00284–0.0287 (0.01%), 0.000896–0.00898 (0.001%) on the $y-$axis. [76]

It is worth noting that larger percent differences like the 1% curve in Fig. (5.2b), which appear rather far from the gravitating body, do not count as viable illustrations of the actual physical setting. Forces here are calculated for a single particle in the box, so naturally, the forces due to neighbouring particles in the real universe do not show in the differences. Moving away from the source, larger percent differences do appear in the current analysis, however, in a muti-particle setup, the force at those points would be sourced dominantly by the neighbouring particles instead, and the force associated with the particle at the origin would be negligible in the first place.

4.2.1 Effect of periodic boundaries on the Yukawa force - revisited

As mentioned earlier, for the concordance cosmological model, periodic boundary conditions result in artificial effects unsupported by theory. It this connection, it appears interesting to see the extent of their influence on force calculations. The relative difference $|(\tilde{F}_{\text{YE}} - \tilde{F}_{\text{Y}})/\tilde{F}_{\text{YE}}|$ is illustrated in Figs. (5.3a) and (5.3b), both of which clearly show that contrary to the previous analysis on periodic forces, the fixed percent differences move away from the body for smaller $\tilde{\lambda}_{\text{eff}}$. The results

also support the conclusions of Sect. (4.1.2), which indicate that using large-enough boxes (which make $\tilde{\lambda}_{\text{eff}}$ smaller) and employing Yukawa gravity in cosmological simulations, impacts of periodicity may be weakened. Table (4.1) provides yet another demonstration of the relationship between the relative difference and the rescaled effective screening length, zooming into four points in the box that are $\tilde{x} = 0.005, 0.01, 0.02$ and 0.2.

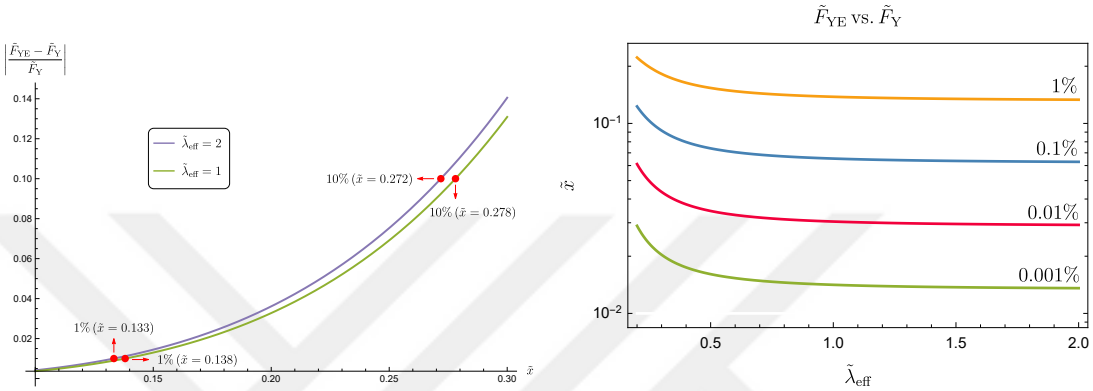

(a) (b)

Figure 4.3 : (a) Relative difference calculated with respect to the x-components of the Yukawa-Ewald and Yukawa forces for $\tilde{\lambda}_{\text{eff}} = 1, 2$ on the $\tilde{y} = \tilde{z} = 0$ line. (b) Locations of four percent differences in the box plotted as functions of $\tilde{\lambda}_{\text{eff}}$ for the $\tilde{F}_{\text{YE}}$ vs. $\tilde{F}_{\text{Y}}$ forces on the $\tilde{y} = \tilde{z} = 0$ line. Moving downwards from the 1% difference, the curves lie between the points 0.222–0.133 (1%), 0.123–0.0628 (0.1%), 0.0611–0.0292 (0.01%), 0.0289–0.0136 (0.001%) on the $y-$axis. [76]

Table 4.1 : Relative difference with respect to the free-boundary (4.9) and periodic Yukawa forces (4.6) at four points in the box when $\tilde{\lambda}_{\text{eff}} = 0.05$ (left chart), 0.1 (middle chart) and 1 (right chart).

$\tilde{\lambda}_{\text{eff}} = 0.005$		$\tilde{\lambda}_{\text{eff}} = 0.1$		$\tilde{\lambda}_{\text{eff}} = 1$	
$\tilde{x}$	$\lvert(\tilde{F}_{\text{YE}} - \tilde{F}_{\text{Y}})/\tilde{F}_{\text{YE}}\rvert$	$\tilde{x}$	$\lvert(\tilde{F}_{\text{YE}} - \tilde{F}_{\text{Y}})/\tilde{F}_{\text{YE}}\rvert$	$\tilde{x}$	$\lvert(\tilde{F}_{\text{YE}} - \tilde{F}_{\text{Y}})/\tilde{F}_{\text{YE}}\rvert$
0.005	2.069×10^{-13}	0.005	1.163×10^{-9}	0.005	4.416×10^{-7}
0.01	1.692×10^{-12}	0.01	9.357×10^{-9}	0.01	3.534×10^{-6}
0.02	1.453×10^{-11}	0.02	7.644×10^{-8}	0.02	2.830×10^{-5}
0.2	1.296×10^{-6}	0.2	4.335×10^{-4}	0.2	0.0327

5. COSMIC SCREENING APPROACH GENERALIZED TO CONTINUOUS MATTER SOURCES

In the presence of an additional perfect fluid with the EMT

$$T^{ik} = (\varepsilon + p)\frac{dx^i}{ds}\frac{dx^k}{ds} - pg^{ik}\,, \tag{5.1}$$

the linearized Einstein equations (3.2)-(3.5) take on the form [2, 3]

$$\triangle\Phi - 3\mathcal{H}\left(\Phi' + \mathcal{H}\Phi\right) = \frac{1}{2}\kappa a^2\left(\frac{c^2}{a^3}\delta\rho + \frac{3\overline{\rho}c^2}{a^3}\Phi + \delta\varepsilon\right)\,, \tag{5.2}$$

$$\begin{aligned}&\frac{1}{4}\triangle B_\alpha + \frac{\partial}{\partial x^\alpha}\left(\Phi' + \mathcal{H}\Phi\right)\\ =\;& \frac{1}{2}\kappa a^2\left(-\frac{c^2}{a^3}\sum_n \rho_n\tilde{v}_n^\alpha + \frac{\overline{\rho}c^2}{a^3}B_\alpha - (\varepsilon + p)\,\tilde{v}^\alpha + (\overline{\varepsilon} + \overline{p})\,B_\alpha\right)\,,\end{aligned} \tag{5.3}$$

$$\Phi'' + 3\mathcal{H}\Phi' + \left(2\mathcal{H}' + \mathcal{H}^2\right)\Phi = \frac{1}{2}\kappa a^2\delta p\,, \tag{5.4}$$

$$\left(\frac{\partial B_\beta}{\partial x^\alpha}\right)' + 2\mathcal{H}\left(\frac{\partial B_\alpha}{\partial x^\beta} + \frac{\partial B_\beta}{\partial x^\alpha}\right) = 0\,, \tag{5.5}$$

given, again, the metric (3.1). In the earlier work [3], ε was separated into two components, ε_I and ε_J, which represented continuous perfect fluids characterized by linear and nonlinear EoS, respectively. Indeed, arbitrary number of such components were allowed, only with the condition that energy density and pressure contrasts of nonlinear perfect fluid(s) were small everywhere: $\delta\varepsilon_J/\overline{\varepsilon}_J, \delta p_J/\overline{p}_J \ll 1$. On the other hand, just like the point-like pressureless matter, the energy density ε_I and pressure p_I of the $\omega_I = \text{const} \neq 0$ components admitted fluctuations of arbitrary magnitude, in agreement with the general scheme of the cosmic screening approach. Peculiar velocities contribute to metric perturbations only through the terms $\propto \rho\tilde{v}_n^\alpha$, $\propto \varepsilon\tilde{v}^\alpha$ and $\propto p\tilde{v}^\alpha$, i.e. when combined with the mass density, energy density and pressure, hence such products appear automatically as first order quantities. In this connection, replacements such as $\varepsilon\tilde{v}^\alpha \to \overline{\varepsilon}\tilde{v}^\alpha$ were omitted contrary to the indispensable substitutions of the form $\rho, \varepsilon, p \times \Phi, B_\alpha \to \overline{\rho}, \overline{\varepsilon}, \overline{p} \times \Phi, B_\alpha$. Situation was, of course, different for the "J"-components with respect to the terms with peculiar velocities: products such as $\varepsilon_J\tilde{v}_J^\alpha, p_J\tilde{v}_J^\alpha$ were replaced by $\overline{\varepsilon}_J\tilde{v}_J^\alpha, \overline{p}_J\tilde{v}_J^\alpha$.

In the case of a linear perfect fluid, the energy density was decomposed as [3]

$$\varepsilon_I = \frac{A_I}{a^{3(1+\omega_I)}} + 3\left(1+\omega_I\right)\overline{\varepsilon}_I\Phi = \frac{\overline{A}_I}{a^{3(1+\omega_I)}} + \frac{\delta A_I}{a^{3(1+\omega_I)}} + \frac{3(1+\omega_I)\overline{A}_I}{a^{3(1+\omega_I)}}\Phi\,, \tag{5.6}$$

so that

$$\overline{\varepsilon}_I = \frac{\overline{A}_I}{a^{3(1+\omega_I)}}\,, \quad \delta\varepsilon_I = \frac{\delta A_I}{a^{3(1+\omega_I)}} + \frac{3(1+\omega_I)\overline{A}_I}{a^{3(1+\omega_I)}}\Phi\,, \tag{5.7}$$

for $\overline{A}_I = \text{const}$ and $A_I = \overline{A}_I + \delta A_I$. Additionally, regarding the "J"-component, it was assumed that

$$\delta\varepsilon_J = \overline{\varepsilon}_J\delta_J + 3\left(\overline{\varepsilon}_J + \overline{p}_J\right)\Phi\,. \tag{5.8}$$

The function δ_J satisfies (2.22) of [3], which follows from the conservation equation of the corresponding fluid in the first-order approximation (given by (2.18) therein).

Using (5.7) and (5.8), Eqs. (5.2) and (5.3) may be rearranged to yield

$$\begin{aligned}
&\triangle\Phi - a^2\left[\frac{3\kappa\overline{\rho}c^2}{2a^3} + \frac{3\kappa}{2}\sum_I\frac{(1+\omega_I)\overline{A}_I}{a^{3(1+\omega_I)}} + \frac{3\kappa}{2}\sum_J\left(\overline{\varepsilon}_J+\overline{p}_J\right)\right]\Phi \\
&= \frac{\kappa c^2}{2a}\delta\rho + \frac{\kappa a^2}{2}\sum_I\frac{\delta A_I}{a^{3(1+\omega_I)}} + \frac{\kappa a^2}{2}\sum_J\overline{\varepsilon}_J\delta_J \\
&-\frac{3\kappa c^2\mathcal{H}}{2a}\Xi - \frac{3\mathcal{H}\kappa}{2}\sum_I\frac{1+\omega_I}{a^{1+3\omega_I}}\xi_I - \frac{3\mathcal{H}\kappa a^2}{2}\sum_J\left(\overline{\varepsilon}_J+\overline{p}_J\right)\zeta_J
\end{aligned} \tag{5.9}$$

for $\varepsilon \to \sum_I \varepsilon_I + \sum_J \varepsilon_J$, $p \to \sum_I p_I + \sum_J p_J$ above and hereafter, and

$$\begin{aligned}
&\frac{1}{4}\triangle\mathbf{B} - \frac{a^2}{3}\left[\frac{3\kappa\overline{\rho}c^2}{2a^3} + \frac{3\kappa}{2}\sum_I\frac{(1+\omega_I)\overline{A}_I}{a^{3(1+\omega_I)}} + \frac{3\kappa}{2}\sum_J\left(\overline{\varepsilon}_J+\overline{p}_J\right)\right]\mathbf{B} \\
&= -\frac{\kappa c^2}{2a}\left(\sum_n\rho_n\tilde{\mathbf{v}}_n - \nabla\Xi\right) - \frac{\kappa}{2}\sum_I\frac{1+\omega_I}{a^{1+3\omega_I}}\left(A_I\tilde{\mathbf{v}}_I - \nabla\xi_I\right) \\
&-\frac{\kappa a^2}{2}\sum_J\left(\overline{\varepsilon}_J+\overline{p}_J\right)\left(\tilde{\mathbf{v}}_J - \nabla\zeta_J\right)\,.
\end{aligned} \tag{5.10}$$

Functions ξ_I and ζ_I are defined via the relations [3]

$$A\tilde{\mathbf{v}}_I = \nabla\xi_I + \left(A_I\tilde{\mathbf{v}}_I - \nabla\xi_I\right)\,, \quad \nabla\left(A_I\tilde{\mathbf{v}}_I\right) = \triangle\xi_I\,, \tag{5.11}$$

$$\tilde{\mathbf{v}}_J = \nabla\zeta_J + \left(\tilde{\mathbf{v}}_J - \nabla\zeta_J\right)\,, \quad \nabla\tilde{\mathbf{v}}_J = \triangle\zeta_J\,. \tag{5.12}$$

Above expressions are obtained by decomposing the velocity-dependent terms into zero-grad and zero-curl pieces. The function ξ_I is interpreted as the *effective velocity potential* of the "I"$-$component, just like the function Ξ defined in (3.10) for point-like nonrelativistic particles and ζ_J are the velocity potentials of nonlinear perfect fluids.

For $\Phi = \Phi_M + \sum_I \Phi_I + \sum_J \Phi_J$, and $\mathbf{B} = \mathbf{B}_M + \sum_I \mathbf{B}_I + \sum_J \mathbf{B}_J$, both (5.9) and (5.10) may be expressed as sets of separate equations for individual components, that are

$$\triangle\Phi_M - \frac{a^2}{\lambda^2}\Phi_M = \frac{\kappa c^2}{2a}\delta\rho - \frac{3\kappa c^2\mathcal{H}}{2a}\Xi\,, \tag{5.13}$$

$$\triangle\Phi_I - \frac{a^2}{\lambda^2}\Phi_I = \frac{\kappa a^2}{2}\frac{\delta A_I}{a^{3(1+\omega_I)}} - \frac{3\mathcal{H}\kappa}{2}\frac{1+\omega_I}{a^{1+3\omega_I}}\xi_I\,, \tag{5.14}$$

$$\triangle\Phi_J - \frac{a^2}{\lambda^2}\Phi_J = \frac{\kappa a^2}{2}\overline{\varepsilon}_J\delta_J - \frac{3\mathcal{H}\kappa a^2}{2}\left(\overline{\varepsilon}_J + \overline{p}_J\right)\zeta_J\,, \tag{5.15}$$

and

$$\frac{1}{4}\triangle\mathbf{B}_M - \frac{a^2}{3\lambda^2}\mathbf{B}_M = -\frac{\kappa c^2}{2a}\left(\sum_n \rho_n\tilde{\mathbf{v}}_n - \nabla\Xi\right)\,, \tag{5.16}$$

$$\frac{1}{4}\triangle\mathbf{B}_I - \frac{a^2}{3\lambda^2}\mathbf{B}_I = -\frac{\kappa}{2}\frac{1+\omega_I}{a^{1+3\omega_I}}\left(A_I\tilde{\mathbf{v}}_I - \nabla\xi_I\right)\,, \tag{5.17}$$

$$\frac{1}{4}\triangle\mathbf{B}_J - \frac{a^2}{3\lambda^2}\mathbf{B}_J = -\frac{\kappa a^2}{2}\left(\overline{\varepsilon}_J + \overline{p}_J\right)\left(\tilde{\mathbf{v}}_J - \nabla\zeta_J\right)\,. \tag{5.18}$$

Naturally, with the addition of extra components in the form of linear and nonlinear perfect fluids, the original screening length introduced in Sect. (3.1) is re-defined and now admits two additional terms for each type of the new components [3]:

$$\lambda = \left[\frac{3\kappa\overline{\rho}c^2}{2a^3} + \frac{3\kappa}{2}\sum_I \frac{(1+\omega_I)\overline{A}_I}{a^{3(1+\omega_I)}} + \frac{3\kappa}{2}\sum_J\left(\overline{\varepsilon}_J + \overline{p}_J\right)\right]^{-1/2}\,. \tag{5.19}$$

The potentials $\Phi_M, \mathbf{B}_M$, $\Phi_I, \mathbf{B}_I$ and $\Phi_J, \mathbf{B}_J$, then, correspond to perturbations sourced by pressureless matter composed of discrete sources (CDM in the form of galaxies, clusters etc.) and by perfect fluids with linear and nonlinear EoS (which may be attributed to the dark energy), respectively.

5.1 Nonlinear Perfect Fluids with Arbitrarily Large Density Contrasts

To enhance the compatibility of the cosmic screening approach with a wider class of models that address the late acceleration of the universe, such as the Chaplygin gas model [77, 78, 79, 80], the set of equations for the scalar and vector potentials were re-considered for nonlinear perfect fluids in the work [5], now for the more general case of arbitrarily large density contrasts.

Herein, the relation $\overline{p}_J = f(\overline{\varepsilon}_J)$ no longer holds as density and pressure fluctuations are not treated as small quantities. Upon introducing a new function $F_J = \overline{F}_J + \delta F_J$,

the energy density of the nonlinear perfect fluid was expressed in [5] as

$$\varepsilon_J = F_J + 3\left(\varepsilon_J + p_J\right)\Phi\,, \tag{5.20}$$

so that for $|\Phi| \ll 1$,

$$\varepsilon_J = F_J + 3\left[F_J + f_J(F_J)\right]\Phi\,, \tag{5.21}$$

$$p_J = f_J(F_J) + 3\frac{\partial f_J}{\partial \varepsilon_J}\bigg|_{\varepsilon_J = F_J}\left[F_J + f_J(F_J)\right]\Phi\,. \tag{5.22}$$

Substituting the above set into the conservation equation ((A.20) in [3]) and rearranging the resulting terms, the following equations were obtained in the background and first order, respectively:

$$\overline{F_J}' + 3\mathcal{H}\left(\overline{F_J} + \overline{f_J(F_J)}\right) = 0\,, \tag{5.23}$$

$$\delta F_J{}' + 3\mathcal{H}\left(\delta F_J + \delta f_J\right) + \nabla\left[\left(F_J + f_J(F_J)\right)\tilde{\mathbf{v}}_J\right] = 0\,. \tag{5.24}$$

In deriving (5.24), certain estimations were taken into consideration such as $\Phi\delta\varepsilon_J/\varepsilon_J \sim \tilde{v}^2$ [81], $c_s^2 = \delta p_J/\delta\varepsilon_J \sim \partial f_J/\partial\varepsilon_J \lesssim 1$, $\delta\varepsilon_J/\varepsilon_J \sim \delta f_J/f_J$, $\delta f_J B \ll f_J\tilde{v}_J$ as well as $\Phi \sim B \sim \tilde{v} \sim \epsilon \ll 1$ at large scales and $\Phi \sim \epsilon,\ B \sim \tilde{v}\Phi$ in small spatial regions. Moreover, the function f_J has been decomposed as $f_J(F_J) = \overline{f_J(F_J)} + \delta f_J$. On the other hand, based on (5.21), the density fluctuation for such component reads

$$\delta\varepsilon_J = \varepsilon_J - \bar{\varepsilon}_J = \delta F_J + 3\left(\overline{F}_J + \overline{f_J(F_J)}\right)\Phi\,. \tag{5.25}$$

Instead of Eq. (5.12) of the previous section, the $\tilde{v}_J^\alpha$ terms were spit into transverse and longitudinal pieces in the form [5]

$$\left(F_J + f_J(F_J)\right)\tilde{\mathbf{v}}_J = \nabla\zeta_{2J} + \left[\left(F_J + f_J(F_J)\right)\tilde{\mathbf{v}}_J - \nabla\zeta_{2J}\right]\,,$$

$$\nabla\left[\left(F_J + f_J(F_J)\right)\tilde{\mathbf{v}}_J\right] = \triangle\zeta_{2J}\,, \tag{5.26}$$

where ζ_{2J} has no analytical solution (neither does ξ_I of (5.11)), but to be treated numerically. Now, according to (5.21), (5.22), (5.25) and (5.1), the Helmholtz equations (5.15) and (5.18) are replaced by the set

$$\triangle\Phi_J - \frac{a^2}{\lambda^2}\Phi_J = \frac{\kappa a^2}{2}\delta F_J - \frac{3\mathcal{H}\kappa a^2}{2}\zeta_{2J}\,, \tag{5.27}$$

$$\frac{1}{4}\triangle\mathbf{B}_J - \frac{a^2}{3\lambda^2}\mathbf{B}_J = -\frac{\kappa a^2}{2}\left[\left(F_J + f_J(F_J)\right)\tilde{\mathbf{v}}_J - \nabla\zeta_{2J}\right]\,, \tag{5.28}$$

where

$$\lambda \equiv \left[\frac{3\kappa}{2}\left(\overline{F}_J + \overline{f_J(F_J)}\right)\right]^{-1/2} \tag{5.29}$$

for a single-component universe. Above equations apply to the general-most case as they are compatible with any $p = f(\varepsilon)$, which also involves the class of linear perfect fluids with density contrasts of arbitrary magnitude. It is important to note that even though they lack analytical solutions, these equations, together with (5.23), (5.24), the background Friedmann equation (i.e. (1) of [5] for the considered component(s)) and the momentum conservation equation ((34) of [5]), serve as a complete set of ready-to-use formulas to be employed in numerical simulations.

6. MULTIDIMENSIONAL $f(R)$ GRAVITY IN THE WEAK-FIELD LIMIT OF KALUZA-KLEIN MODELS

Einstein field equations for $f(R)$ gravity in $\mathcal{D} = 1 + D \geq 4$ dimensional spacetime have the form [21, 22, 23]

$$\begin{aligned} f'(R)R_{ik} - \frac{1}{2}f(R)g_{ik} - [f'(R)]_{;i;k} + g_{ik}\,[f'(R)]_{;m;n}\,g^{mn} &= \frac{2S_D\tilde{G}_{\mathcal{D}}}{c^4}T_{ik}\,, \\ i,k &= 0,1,...,D\,, \end{aligned} \quad (6.1)$$

where D is the number of spatial dimensions and the total solid angle $S_D = 2\pi^{D/2}/\Gamma(D/2)$. $\tilde{G}_{\mathcal{D}}$ represents the $\mathcal{D}$-dimensional gravitational constant, $' \equiv d/dR$ for $R = R_{ik}g^{ik}$ and the semicolon indicates covariant derivatives with respect to coefficients g_{ik} of the metric

$$ds^2 = g_{00}\left(dx^0\right)^2 + 2g_{0\alpha}dx^0dx^a + g_{\alpha\beta}dx^\alpha dx^\beta\,, \quad \alpha,\beta = 1,2,...,D\,. \quad (6.2)$$

In the absence of background matter, the unperturbed spacetime with d-dimensional internal compact space has a flat metric and may be assigned a topology $\mathbb{R}\times\mathbb{R}^3\times T^d$ [27, 28, 37, 82, 83, 84]. A curved background geometry, on the other hand, is possible when there is matter present and in the $(D = 3 + d)$-dimensional KK models with spherical compactification of the internal space, it admits a topology $\mathbb{R}\times\mathbb{R}^3\times S^d$ [29, 30, 31, 41, 42]. For static background metrics, as in the current configuration, $g^{(0)}_{0\alpha} = 0$ so in the latter case, the EMT of the background matter reads

$$\left(T^i_k\right)^{(0)} = \mathrm{diag}\left(\overline{\varepsilon}, -\overline{p}_0, -\overline{p}_0, -\overline{p}_0, \underbrace{-\overline{p}_1, ..., -\overline{p}_1}_{d-\mathrm{times}}\right)\,. \quad (6.3)$$

The overline as well as zero superscripts indicate background quantities. Employing (6.1) at the background level, one obtains $\overline{\omega}_0 \equiv \overline{p}_0/\overline{\varepsilon} = -1$ and the parameter $\overline{\omega}_1 \equiv \overline{p}_1/\overline{\varepsilon}$ of the internal space may be determined once the form of $f(R)$ is specified.

Introducing a static point-like mass induces slight perturbations in the background metric so that the coefficients in (6.2) take on the form $g_{ik} \approx g^{(0)}_{ik} + h_{ik}$, where h_{ik} stand for small corrections of the order $1/c^2$. From this point on, the first-order metric

corrections will be denoted by A^1, B^1 and G^1 and the number of extra dimensions will be limited to two for simpler demonstration:

$$ds^2 = \left(1 + A^1\right) c^2 dt^2 - (1 - B^1) \sum_{\alpha=1}^{3} \left(dx^\alpha\right)^2 - \left(1 - G^1\right) \left(d\xi^2 + d\zeta^2\right) \tag{6.4}$$

on the product manifold $M = \mathbb{R} \times \mathbb{R}^3 \times T^2$ and

$$ds^2 = \left(1 + A^1\right) c^2 dt^2 - (1 - B^1) \sum_{\alpha=1}^{3} \left(dx^\alpha\right)^2 - \left(b^2 - G^1\right) \left(d\xi^2 + \sin^2 \xi d\zeta^2\right) \tag{6.5}$$

on $M = \mathbb{R} \times \mathbb{R}^3 \times S^2$. The constant b denotes the radius of the sphere describing internal space. As will be presented explicitly below, the pressure associated with this massive body is isotropic in each of the individual factor manifolds. Therefore, the block-diagonal form of the background metric tensor is unaltered by perturbations [41] in (6.4) and (6.5), where $h_{11} = h_{22} = h_{33} = B^1$ and $h_{44} = h_{55} = G^1$.

Provided that the gravitating source is uniformly smeared over the extra dimensions, its mass density reads $\hat{\rho}(r_3) = m\delta(\mathbf{r}_3)/V_{\text{int}}$ (ensuring $g_{ik} = g_{ik}(r_3)$, $r_3 = |\mathbf{r}_3| = \sqrt{(x^1)^2 + (x^2)^2 + (x^3)^2}$ for spherically symmetric perturbations with respect to the external space [85]). In the flat background, internal space volume $V_{\text{int}} = \Pi_{i=1}^{2} b_i$, where b_i are periods of the tori and as for the compactification on S^2, $V_{\text{int}} = 4\pi b^2$, which corresponds to the surface area of the 2-sphere. In the external space, the source obeys a dust-like EoS, as is typical of astrophysical objects with weak gravitational fields. The EoS parameter in the internal space remains unspecified, so one treats the corresponding parameter Ω as a free parameter of the model. The nonzero components of the EMT are, then, approximated as

$$\hat{T}_0^0 \approx \hat{\rho} c^2 \,, \quad \hat{T}_\nu^\mu \approx -\delta_\nu^\mu \Omega \hat{\rho} c^2 \,, \quad \mu, \nu = 4, 5 \tag{6.6}$$

within the adopted accuracy.

Taking into consideration the fluctuations of the scalar curvature R, which may be decomposed in terms of the background contribution and the first order correction, respectively, as $R = R_0 + R_1$, the function $f(R)$ is Taylor- expanded about R_0:

$$\begin{aligned} f(R) &= f(R_0) + f'(R_0) R_1 + \mathcal{O}\left(R_1^2\right) \,, \\ f'(R) &= f'(R_0) + f''(R_0) R_1 + \mathcal{O}\left(R_1^2\right) \,. \end{aligned} \tag{6.7}$$

The LHS of the field equations (6.1) are then determined in the first-order using (6.4) (or (6.5)) together with (6.7). Eventually, these equations are to be solved for the metric

perturbations A^1, B^1 and G^1. The first-order contribution to the RHS of (6.1) comes not only from (6.6), but also from the nonzero elements of the perturbed background EMT - of course, only when the model includes background matter - that are

$$\delta T^0_0 \approx \delta\varepsilon\,, \quad \delta T^\alpha_\beta \approx -\delta p_0 \delta^\alpha_\beta\,, \quad \delta T^\mu_\nu \approx -\delta p_1 \delta^\mu_\nu\,. \tag{6.8}$$

Through (6.8), the model admits two more free parameters $\omega_0 \equiv \delta p_0/\delta\varepsilon$ and $\omega_1 \equiv \delta p_1/\delta\varepsilon$.

The first coefficient A^1 represents the gravitational potential, therefore it is natural to expect that in the limit $(r_3 \to \infty)$, it would take on the Newtonian form, i.e. $A^1(r_3 \to \infty) = -2G_N m/(c^2 r_3)$. This condition defines the relation between constants $\tilde{G}_{\mathcal{D}}$ and G_N in terms of the free parameters.

In comparison to (6.4) and (6.5), the form the static, spherically symmetric metric [39, 40]

$$ds^2 = \left(1 - \frac{2G_N m}{c^2 r}\right) c^2 dt^2 - \left(1 + \gamma \frac{2G_N m}{c^2 r}\right) \sum_{i=1}^{3} \left(dx^i\right)^2 \tag{6.9}$$

in PPN formalism implies $\gamma = B^1/A^1$. To achieve good agreement with observational constraints from solar system tests of gravity, this ratio should be equal to one as in GR. Such requirement serves as a tool to determine the viable combinations of the free parameters which appear in the expressions for B^1 and A^1.

Evidently, the scheme applies also to the study of linear models (which correspond to the particular case of $f''(R) = 0$) and one may as well investigate a more general model in which the extra dimensions consist of multiple product spaces.

6.1 The $d = 2$ Case in the Presence of a Nonlinear Background Fluid

Assuming a perfect fluid in the background, with the EMT in (6.3) for $d = 2$, and thus for the metric (6.5), linearized field equations from (6.1) may be cast into the form

$$00- \qquad \frac{f'(R_0)}{2}\left(\Delta_3 A^1 - R_1\right) - \left(\Delta_3 R_1\right) f''(R_0) = \kappa\left(\delta\varepsilon + \hat{\rho}c^2\right)\,, \tag{6.10}$$

$$\alpha\alpha- \qquad \frac{f'(R_0)}{2}\left(\Delta_3 B^1 + R_1\right) + \left(\Delta_3 R_1\right) f''(R_0) = \kappa\delta p_0\,, \tag{6.11}$$

$$\mu\mu- \qquad \frac{f'(R_0)}{2}\left(\Delta_3\frac{2G^1}{b^2}+2R_1\right)+f''(R_0)\frac{2R_1}{b^2}+2\left(\Delta_3 R_1\right)f''(R_0)$$
$$=-f'(R_0)\frac{2G^1}{b^4}+2\kappa\left(\delta p_1+\Omega\hat{\rho}c^2\right)\,, \tag{6.12}$$
$$\alpha\beta- \qquad \frac{1}{2}f'(R_0)\left(-A^1+B^1+2\frac{G^1}{b^2}\right)-f''(R_0)R_1=0 \tag{6.13}$$

upon introducing a point mass with the previously discussed properties (up to the replacement $r_3 \to r$ for notation-wise consistency with the work [86]). Of course, it has been taken into consideration that metric perturbations and the scalar curvature all tend to zero as $r \to \infty$.

A useful expression may be obtained by combining the equations in the set above, that is

$$5f''(R_0)(\Delta_3 R_1)+2f'(R_0)R_1+\frac{2}{b^2}f''(R_0)R_1$$
$$=\quad -f'(R_0)\frac{2G^1}{b^4}+\kappa\left[-\delta\varepsilon+\delta p_0+2\delta p_1-\hat{\rho}c^2(1-2\Omega)\right]\,. \tag{6.14}$$

The trace of (6.1) for this configuration follows as

$$-\quad 2f'(R_0)R_1+f''(R_0)\left(R_0R_1-5\Delta_3R_1\right)$$
$$=\kappa\left[\delta\varepsilon-3\delta p_0-2\delta p_1+\hat{\rho}c^2(1-2\Omega)\right]\,, \tag{6.15}$$

which, when combined with (6.14), provides an expression that relates δp_0 of the perfect fluid to the metric coefficient G^1:

$$\delta p_0=-\frac{f'(R_0)}{\kappa b^4}G^1\,. \tag{6.16}$$

In the external and internal spaces, the squared speed of sound for the perfect fluid are defined via $\delta p_0=\omega_0\delta\varepsilon$ and $\delta p_1=\omega_1\delta\varepsilon$, respectively, so that (6.16) also implies

$$\delta\varepsilon=-\frac{f'(R_0)}{\kappa b^4}\frac{1}{\omega_0}G^1\,,\quad \delta p_1=-\frac{f'(R_0)}{\kappa b^4}\frac{\omega_1}{\omega_0}G^1\,,\quad \omega_0\neq 0\,. \tag{6.17}$$

Substituting (6.16) and (6.17) in Eqs. (6.10)-(6.12), one obtains the set of master equations

$$\frac{f'(R_0)}{2}\Delta_3B^1+\frac{f'(R_0)}{2}R_1+f''(R_0)\Delta_3R_1+\frac{f'(R_0)}{b^4}G^{=}0\,, \tag{6.18}$$
$$\frac{f'(R_0)}{2}\Delta_3A^1-\frac{f'(R_0)}{2}R_1-f''(R_0)\Delta_3R_1+\frac{f'(R_0)}{b^4}\frac{1}{\omega_0}G^1=\kappa\hat{\rho}c^2\,, \tag{6.19}$$
$$\frac{f'(R_0)}{2b^2}\Delta_3G^1+\frac{f'(R_0)}{2}R_1+\frac{f''(R_0)}{b^2}R_1$$
$$+f''(R_0)\Delta_3R_1+\frac{f'(R_0)}{b^4}\left(1+\frac{\omega_1}{\omega_0}\right)G^1=\kappa\Omega\hat{\rho}c^2\,, \tag{6.20}$$

which, together with Eq. (6.13) is to be solved for the metric coefficients A^1, B^1, G^1 and the curvature perturbation R^1 (see Sect. (2) of [86] for an explicit derivation of Eqs. (6.10)-(6.13) and (6.15)).

The perfect fluid responsible for the curved background geometry is chosen to be nonlinear, which means, $\omega_0 \neq \overline{\omega}_0$ and $\omega_1 \neq \overline{\omega}_1$. At this point, it is also worth noting that the equations derived in this section require $f'(R_0) \neq 0$. To avoid the ghost graviton, negative values of this function should also be eliminated so that the constraint becomes $f'(R_0) > 0$.

6.1.1 Solutions for the perturbation variables

It has been shown in [86] that the solutions for the generic setup $f''(R_0) \neq 0, \overline{\omega}_0 \neq 0$ need to be worked out for two distinct cases, that is, when the Yukawa masses μ_1 and μ_2 are different from one another and when the solutions admit a single Yukawa mass. For the former, the analytical solutions have been found as

$$A^1(r) = \sqrt{\frac{\pi}{2}}\frac{1}{r}\left[\beta_3 + \beta_{1A}\exp\left(-\mu_1 r\right) + \beta_{2A}\exp\left(-\mu_2 r\right)\right] , \tag{6.21}$$

$$B^1(r) = \sqrt{\frac{\pi}{2}}\frac{1}{r}\left[\beta_3 + \beta_{1B}\exp\left(-\mu_1 r\right) + \beta_{2B}\exp\left(-\mu_2 r\right)\right] , \tag{6.22}$$

$$G^1(r) = \sqrt{\frac{\pi}{2}}\frac{1}{r}\left[\beta_{1G}\exp\left(-\mu_1 r\right) + \beta_{2G}\exp\left(-\mu_2 r\right)\right] , \tag{6.23}$$

$$R^1(r) = \sqrt{\frac{\pi}{2}}\frac{1}{r}\left[\beta_{1R}\exp\left(-\mu_1 r\right) + \beta_{2R}\exp\left(-\mu_2 r\right)\right] , \tag{6.24}$$

where the parameters β_X are given by (37), (38), (40), (41) and (45) of [86] and

$$\begin{aligned}\mu_{1,2} = \frac{1}{\sqrt{5}}\frac{1}{b}\Bigg[&-b^2\frac{f'(R_0)}{f''(R_0)} - \frac{(1+3\omega_0+3\omega_1)}{\omega_0} \\ &\mp\frac{1}{f''(R_0)\omega_0}\Big[b^4 f'^2(R_0)\omega_0^2 + b^2 f'(R_0)f''(R_0)(-3+\omega_0-4\omega_1)\omega_0 \\ &+ f''^2(R_0)\left(19\omega_0^2 + 2\omega_0(-2+9\omega_1) + (1+3\omega_1)^2\right)\Big]^{1/2}\Bigg]^{1/2} .\end{aligned} \tag{6.25}$$

From (6.21) and (6.22), one immediately sees that $A^1(r\to\infty) = B^1(r\to\infty)$. The corresponding expression is given by [86]

$$\begin{aligned}A^1(r\to\infty) = &-\frac{2}{c^2}\frac{1}{4\pi}\frac{S_D\tilde{G}_{\mathcal{D}}}{V_{\rm int}}\frac{m}{r} \\ \times\quad &\frac{2f'(R_0)b^2\left[\Omega(1+\omega_0)-\omega_1\right] + 4f''(R_0)\omega_0}{f'(R_0)\left[2f''(R_0)(\omega_0-1) - b^2 f'(R_0)(1+\omega_0+2\omega_1)\right]} .\end{aligned} \tag{6.26}$$

As the metric perturbation A^1 represents the gravitational potential [38], it is natural to expect that $A^1(r \to \infty) = -2G_N m/c^2 r$, which helps in determining the relation between $\tilde{G}_{\mathcal{D}}$ and the Newtonian gravitational constant G_N:

$$\frac{S_D \tilde{G}_{\mathcal{D}}}{V_{\rm int}} \frac{2f'(R_0)b^2\left[\Omega(1+\omega_0)-\omega_1\right]+4f''(R_0)\omega_0}{f'(R_0)\left[2f''(R_0)(\omega_0-1)-b^2 f'(R_0)(1+\omega_0+2\omega_1)\right]} = 4\pi G_N \,. \tag{6.27}$$

6.1.2 The $f(R) = R + \xi R^2$ example for $\mu_1 \neq \mu_2$

For the particular example $f(R) = R + \xi R^2$, the previously introduced constraint $f'(R_0) > 0$ requires $b^2 > 4\xi$. Considering the case $|\xi| \sim b^2$, it has been found that the masses μ_1, μ_2, which have the general form

$$\begin{aligned} \mu_{1,2} = \frac{1}{\sqrt{10}}\frac{1}{b}\Bigg[& -\frac{b^2}{\xi} - \frac{2(1+\omega_0+3\omega_1)}{\omega_0} \\ \mp & \frac{1}{\xi\omega_0}\left[b^4\omega_0^2 - 2b^2\xi(3+3\omega_0+4\omega_1)\omega_0\right. \\ + & \left. 4\xi^2\left(21\omega_0^2+\omega_0(2+26\omega_1)+(1+3\omega_1)^2\right)\right]^{1/2}\Bigg]^{1/2} , \end{aligned} \tag{6.28}$$

become $\sim 1/b$ provided that $\omega_0, \omega_1 \sim \mathcal{O}(1)$. The scalaron [27] and radion masses are also $\sim 1/b$ for $|\xi| \sim b^2$:

$$m_{\rm rad} \sim 1/b \,, \tag{6.29}$$

$$m_{\rm scal} = \frac{1}{\sqrt{5}}\left(-\frac{2f'(R_0)}{f''(R_0)} + R_0\right)^{1/2} = \frac{1}{\sqrt{5|\xi|}}\left(\frac{2|\xi|}{b^2} - \frac{|\xi|}{\xi}\right)^{1/2} . \tag{6.30}$$

Same relations hold when $|\xi| \gg b^2$ (and $\omega_0, \omega_1 \sim \mathcal{O}(1)$), for which the full form of Yukawa masses read [86]

$$\begin{aligned} \mu_{1,2} \approx & \frac{1}{\sqrt{5}}\frac{1}{b} \\ \times & \left[-\frac{(1+\omega_0+3\omega_1)}{\omega_0} \mp \frac{|\xi|}{\xi}\frac{1}{\omega_0}\left[21\omega_0^2+(2+26\omega_1)\omega_0+(1+3\omega_1)^2\right]^{1/2}\right]^{1/2} . \end{aligned} \tag{6.31}$$

On the other hand, in the limit $|\xi| \ll b^2$, $m_{\rm scal} \sim (-1/\xi)^{1/2}$ for $\xi < 0$, and [86]

$$\mu_{1,2} \approx \frac{1}{\sqrt{10}}\frac{1}{b}\left[-\frac{b^2}{\xi} \mp \frac{|\omega_0|}{\omega_0}\frac{b^2}{\xi}\left(1 - \frac{\xi}{b^2}\frac{3+3\omega_0+4\omega_1}{\omega_0}\right)\right]^{1/2} . \tag{6.32}$$

Proceeding with the negative values of the parameter ω_0, (6.32) yields

$$\mu_1 \approx \frac{1}{\sqrt{10}}\frac{1}{b}\left(-\frac{3+3\omega_0+4\omega_1}{\omega_0}\right)^{1/2} \sim \frac{1}{b} \sim m_{\rm rad} \,, \tag{6.33}$$

$$\mu_2 \approx \frac{1}{\sqrt{5}}\frac{1}{b}\left(-\frac{b^2}{\xi}\right)^{1/2} = \frac{1}{\sqrt{5|\xi|}} \approx m_{\rm scal} \tag{6.34}$$

As follows from the above set as well as the condition $\sqrt{|\xi|} \ll b$, the exponential terms $\propto \exp(-\mu_2 r)$ in (6.21)-(6.24) may be dropped and left with a single Yukawa term, one may employ the results of ISL experiments to estimate a lower limit for μ_1 (under, of course, some assumptions on the orders of the free parameters contained in the coefficient β_{1A} of (6.21)).

Now, from $\mu_1(b \to \infty) = 0$, and $\mu_2(b \to \infty) = m_{\rm scal} = \sqrt{-1/(5\xi)}$, one obtains [86]

$$A^1(r) = \sqrt{\frac{\pi}{2}}\frac{1}{r}\kappa' \left[-\frac{2\Omega + 3}{2} + \frac{(2\Omega - 1)}{10} \exp\left(-\mu_2 r\right) \right] , \tag{6.35}$$

$$B^1(r) = \sqrt{\frac{\pi}{2}}\frac{1}{r}\kappa' \left[\frac{2\Omega - 1}{2} + \frac{(1 - 2\Omega)}{10} \exp\left(-\mu_2 r\right) \right] , \tag{6.36}$$

which straightforwardly show that in order to restore $A^1(r \to \infty) = B^1(r \to \infty)$, one should set $\Omega = -1/2$, and thereby, $S_D \tilde{G}_{\mathcal{D}}/V_{\rm int} = 4\pi G_N$.

6.1.3 $f(R) = R + \xi R^2$ revisited for the degenerate case

When there is a single Yukawa mass, i.e. for $\mu_1 = \mu_2 = \mu$ in (42) of [86], instead of the set (6.21)-(6.24), one obtains

$$A^1(r) = \sqrt{\frac{\pi}{2}}\frac{1}{r} \left[\gamma_3 + \left(\gamma_{1A} + \frac{r}{2\mu}\gamma_{2A} \right) \exp\left(-\mu r\right) \right] , \tag{6.37}$$

$$B^1(r) = \sqrt{\frac{\pi}{2}}\frac{1}{r} \left[\gamma_3 + \left(\gamma_{1B} + \frac{r}{2\mu}\gamma_{2B} \right) \exp\left(-\mu r\right) \right] , \tag{6.38}$$

$$G^1(r) = \sqrt{\frac{\pi}{2}}\frac{1}{r} \left(\gamma_{1G} + \frac{r}{2\mu}\gamma_{2G} \right) \exp\left(-\mu r\right) , \tag{6.39}$$

$$R_1(r) = \sqrt{\frac{\pi}{2}}\frac{1}{r} \left(\gamma_{1R} + \frac{r}{2\mu}\gamma_{2R} \right) \exp\left(-\mu r\right) , \tag{6.40}$$

where the coefficients γ_X in (6.37)-(6.40) are given by (75) of [86], and

$$\mu = \sqrt{\frac{\alpha_5}{2\alpha_4}} = \sqrt{-\frac{1}{5}\left(\frac{f'(R_0)}{f''(R_0)} + \frac{(1 + 3\omega_0 + 3\omega_1)}{b^2\omega_0} \right)} . \tag{6.41}$$

Substituting $f(R) = R + \xi R^2$, the Yukawa mass becomes

$$\mu = \frac{1}{\sqrt{|\xi|}} \left(-\frac{|\xi|}{b^2}\frac{1 + \omega_0 + 3\omega_1}{5\omega_0} - \frac{1}{10}\frac{|\xi|}{\xi} \right)^{1/2} . \tag{6.42}$$

Re-considering the limiting cases in the previous section, one finds the relations

$$\mu \approx \frac{1}{b} \left(\frac{1 + \omega_0 + 3\omega_1}{-5\omega_0} \right)^{1/2} \sim m_{\rm scal} \sim m_{\rm rad} \sim \frac{1}{b} , \tag{6.43}$$

$$m_{\rm scal} \sim 1/\sqrt{|\xi|},\, \xi < 0\,, \quad \mu \approx \sqrt{\frac{1}{10|\xi|}} \sim m_{\rm scal}\,, \tag{6.44}$$

for $|\xi| \gg b^2$ and $|\xi| \ll b^2$, respectively.

6.1.4 The cases with $f''(R_0 = 0)$, $\omega_0 \neq 0$ and the linear model $f(R) = R + 2\kappa\Lambda_6$

Imposing $f'(R_0) \neq 0$, metric perturbations for models with $f''(R_0 = 0), \omega_0 \neq 0$ take on the form

$$A^1(r) = \sqrt{\frac{\pi}{2}}\frac{1}{r}\left[\frac{\alpha_3}{\alpha_6} + \left(\frac{\alpha_{2A}}{\alpha_5} - \frac{\alpha_3}{\alpha_6}\right)\exp\left(-\mu r\right)\right]\,, \tag{6.45}$$

$$B^1(r) = \sqrt{\frac{\pi}{2}}\frac{1}{r}\left[\frac{\alpha_3}{\alpha_6} + \left(\frac{\alpha_{2B}}{\alpha_5} - \frac{\alpha_3}{\alpha_6}\right)\exp\left(-\mu r\right)\right]\,, \tag{6.46}$$

$$G^1(r) = \sqrt{\frac{\pi}{2}}\frac{1}{r}\left[\left(\frac{\alpha_{2G}}{\alpha_5}\right)\exp\left(-\mu r\right)\right]\,, \tag{6.47}$$

$$R_1(r) = (2\pi)^{3/2}\delta(\mathbf{r})\frac{\alpha_{1R}}{\alpha_5} + \sqrt{\frac{\pi}{2}}\frac{1}{r}\left[\left(\frac{\alpha_{2R}}{\alpha_5} - \frac{\alpha_{1R}}{\alpha_5}\cdot\frac{\alpha_6}{\alpha_5}\right)\exp\left(-\mu r\right)\right]\,. \tag{6.48}$$

Specifying the value of the non-vanishing first derivative, i.e., setting $f'(R_0) = 1$, one may perform a more detailed analysis on a specific group of models which also include $f(R) = R + 2\kappa\Lambda_6$. In this case, the above set becomes

$$A^1(r) = \sqrt{\frac{\pi}{2}}\frac{1}{r}\kappa'\left\{\frac{2\left[\Omega(1+\omega_0)-\omega_1\right]}{(1+\omega_0+2\omega_1)} - \left[\frac{3+2\Omega}{2} + \frac{2\left[\Omega(1+\omega_0)-\omega_1\right]}{(1+\omega_0+2\omega_1)}\right] \times \exp\left(-\sqrt{-\frac{1}{2}\frac{(1+\omega_0+2\omega_1)}{\omega_0}}\frac{r}{b}\right)\right\}\,, \tag{6.49}$$

$$B^1(r) = \sqrt{\frac{\pi}{2}}\frac{1}{r}\kappa'\left\{\frac{2\left[\Omega(1+\omega_0)-\omega_1\right]}{(1+\omega_0+2\omega_1)} - \left[\frac{1-2\Omega}{2} + \frac{2\left[\Omega(1+\omega_0)-\omega_1\right]}{(1+\omega_0+2\omega_1)}\right] \times \exp\left(-\sqrt{-\frac{1}{2}\frac{(1+\omega_0+2\omega_1)}{\omega_0}}\frac{r}{b}\right)\right\}\,, \tag{6.50}$$

$$G^1(r) = -\sqrt{\frac{\pi}{2}}\frac{1}{r}\kappa' b^2\left(\frac{1}{2}+\Omega\right)\exp\left(-\sqrt{-\frac{1}{2}\frac{(1+\omega_0+2\omega_1)}{\omega_0}}\frac{r}{b}\right)\,, \tag{6.51}$$

$$R_1(r) = -\kappa'(2\pi)^{3/2}\delta(\mathbf{r})\left(\frac{1}{2}-\Omega\right) + \sqrt{\frac{\pi}{2}}\frac{1}{r}\kappa'\left[\frac{(2\omega_1+3\omega_0-1)(1+2\Omega)}{4b^2\omega_0}\exp\left(-\sqrt{-\frac{1}{2}\frac{(1+\omega_0+2\omega_1)}{\omega_0}}\frac{r}{b}\right)\right]\,. \tag{6.52}$$

For $\omega_0 = \overline{\omega}_0 = -1$, $\omega_1 = \overline{\omega}_1 = \Lambda_6/[1/(\kappa b^2) - \Lambda_6]$, one exactly recovers $f(R) = R + 2\kappa\Lambda_6$, and now $A^1(r \to \infty) = B^1(r \to \infty)$ indicates

$$\frac{S_D \tilde{G}_{\mathcal{D}}}{V_{\text{int}}} \frac{2\left[-\Omega(1+\omega_0)+\omega_1\right]}{(1+\omega_0+2\omega_1)} = \frac{S_D \tilde{G}_{\mathcal{D}}}{V_{\text{int}}} = 4\pi G_N \,. \tag{6.53}$$

For the form of A^1 in (6.49), ISL experiments set an upper bound of $\sim 10^{-3}\,\text{cm}$ for the internal space radius provided that $\omega_0 = -1$ and that one makes the reasonable assumption $|\Omega|, \omega_1 \sim \mathcal{O}(1)$. This shows that at distances comparable to the radius of the Sun, which is $\sim 10^{10}$ cm, the Yukawa contribution may be neglected safely.

Meanwhile, the particular EoS $\Omega = -1/2$ (accompanied by the condition $\omega_0 \neq 0$ and taking into consideration (6.53)) yields $A^1(r) = B^1(r) = -2G_N m/c^2 r$, as the Yukawa corrections vanish immediately owing to zero prefactors.

7. CONCLUSIONS

In this thesis, an extensive study on gravitational interactions has been presented in the cosmological setting and within the framework of the cosmic screening approach [1, 2, 3, 4, 5, 6, 10, 11, 12, 13, 14], which provides a general relativistic formulation for all-scale cosmological perturbations.

First, Helmholtz equations of discrete cosmology and relativistic perturbation theory for the scalar potential have been combined to obtain the effective screening length [10], which corresponds to the cutoff range of Yukawa-type interactions, equal to $2.57\ \mathrm{Gpc}$ today for the ΛCDM model. The novel Helmholtz equation is reduced to the Poisson equation at small-enough scales, incorporates the contribution of peculiar velocities essential to large-scale dynamics, and via the effective screening length, introduces an upper bound for dimensions of distinct cosmic structures. Unlike the previously suggested values for the scale of homogeneity of the order of few hundred Mpc (e.g, as in [87]), the $2.57\ \mathrm{Gpc}$ interaction range coincides with the size of the largest cosmic structure observed, Her-CrB GW, with reported dimensions of $2-3\,\mathrm{Gpc}$ [61, 62]. This supports the argument that the effective screening length of combined approaches defines the bounds of the domain in which structures may grow.

Later on, the novel approach has been adapted to spaces with nonzero curvature [11], and analytical expressions for the scalar potential have been obtained for open and closed universes together with the formula for the effective screening length, which was identical in form to its counterpart in the flat universe [10].

A comparison of the free-boundary and periodic Newtonian forces was performed previously in [15] to mark the distances at which a notable deviation took place in the box from the gravitating source. In [76], Yukawa and Newtonian forces have been studied for a single particle in the cubic periodic domain to reveal that a relative difference of 0.001% already took place at a distance less than 1% of the box size. In a $1.3\,\mathrm{Gpc}$ box today, this corresponded to a distance of $12\,\mathrm{Mpc}$. The relative difference point got closer to the gravitating body moving back into the matter-dominated epoch,

towards the redshift $z = 119$. In the same setting, and based on the formulae presented in [12] for the gravitational potential in the T^3 topology, the impact of periodic boundaries on the Yukawa force has been analyzed and it has been revealed that when the ratio of the effective screening length to the dimensions of the box is kept small-enough, effects of periodicity showed less in the calculations.

The cosmic screening approach was initially introduced in [1], where the sources of the inhomogeneous gravitational field were considered to be discrete delta-shaped bodies-only. In the following work [2, 3] the scheme was extended to include perfect fluids with linear and nonlinear EoS, however, density contrasts of the latter components were considered to be small everywhere. Within the scope of this thesis, the Helmholtz equations for the scalar and vector potentials were revisited for the case where energy density and pressure contrasts of nonlinear perfect fluids were allowed to approach the order of unity $\delta \sim 1$, which is crucial to formulating interactions at small distances. Consequently, a complete set of formulas has been presented in [5], which may be employed in cosmological simulations to study a variety of models that address the accelerated expansion of the universe, like, for instance, the Chaplygin gas model [77, 78, 79, 80].

Finally, in the higher-dimensional setting, Yukawa corrections in nonlinear $f(R)$ models have been studied within the framework of KK models with spherical compactification of the $d = 2$ dimensional internal space [86]. For some nonlinear perfect fluid in the background, responsible for the curved geometry, it has been shown that metric perturbations admitted correction terms which consisted of two summed Yukawa potentials with characteristic ranges $\mu_{1,2}^{-1}$. The point-like source perturbing the background had zero pressure in the external space and some EoS Ω in the internal space that was initially unspecified.

For the specific case $f(R) = R+\xi R^2$, the relationship between $\mu_{1,2}$ and the two scalar degrees of freedom [22, 32, 33, 34, 35] inherent in multidimensional and nonlinear $f(R)$ models have been explored for certain limiting cases. The explicit expression for the higher dimensional gravitational constant has been specified in terms of G_N and the free parameters in the setup. Explicit forms of metric corrections have been presented also for the degenerate case $\mu_1 = \mu_2 = \mu$ for the generic model $f''(R_0) \neq 0$ and a similar analysis has been performed considering the example $f(R) = R + \xi R^2$.

As for the models $f''(R_0) = 0$, effects of the nonlinear background perfect fluid have been investigated and it has been deduced that an agreement with Solar system tests may be achieved either for large-enough values of $m_{\rm rad} \sim 1/b$, where b is the internal space radius and $m_{\rm rad}$ is the scalar degree of freedom associated with multidimensional models, with arbitrary Ω, or for $\Omega = -1/2$ with arbitrary $m_{\rm rad}$.

In future work, first and foremost, it would be an interesting task to adapt the available codes of cosmological simulations to the scheme of *screening* to perform various analyses as in [88]. Then, elaborating further on the combined approach introduced in Sect. (3), one could also extend the formulation to cover the second-order theory, as was done for the original screening approach in [89, 90]. Spatial averages of potential expressions presented in this thesis vanish in the first order. However, in the second-order, nonzero average values of metric perturbations provoke backreaction effects (see, e.g. [91, 92, 93, 94, 95]), due to which a disparity arises between the background universe described by the FRW metric and the *actual* description of spacetime and matter at the zero-th order. For that reason, it appears a particularly nontrivial task to verify to what extent the second-order order quantities contribute to the overall perturbative scheme and whether the formulation may be limited to first-order in the absence of backreaction to a good approximation. Additionally, higher-order velocity contributions could be taken into consideration in the next steps so that the observable effects of relativistic species on the large-scale structure may be also addressed.

REFERENCES

[1] **Eingorn, M.** (2016). First-order cosmological perturbations engendered by point-like masses, *Astrophys. J.*, *825*, 84.

[2] **Eingorn, M. and Brilenkov, R.** (2017). Perfect fluids with $\omega = \mathrm{const}$ as sources of scalar cosmological perturbations, *Phys. Dark Univ.*, *17*, 63.

[3] **Eingorn, M., Kiefer, C. and Zhuk, A.** (2016). Scalar and vector perturbations in a universe with discrete and continuous matter sources, *J. Cosmol. Astropart. Phys.*, *09*, 032.

[4] **Eingorn, M., Kiefer, C. and Zhuk, A.** (2017). Cosmic screening of the gravitational interaction, *Int. J. Mod. Phys. D*, *26*, 1743012.

[5] **Canay, E., Brilenkov, R., Eingorn, M., Arapoğlu, A.S. and Zhuk, A.** (2021). Scalar and vector perturbations in a universe with nonlinear perfect fluid, *Eur. Phys. J. C*, *81*, 246.

[6] **Eingorn, M., Yükselci, A.E. and Zhuk, A.** (2019). Effect of the spatial curvature of the Universe on the form of the gravitational potential, *Eur. Phys. J. C*, *79*, 655.

[7] **Akarsu, Ö., Brilenkov, R., Eingorn. M., Shulga, V. and Zhuk, A.** (2018). Scalar perturbations in cosmological f(R) models: the cosmic screening approach, *Eur. Phys. J. C*, *78*, 609.

[8] **Bhattacharya, S., Kousvos, S.R., Romanopoulos S. and Tomaras, T.N.** (2018). Cosmological screening and the phantom braneworld model, *Eur. Phys. J. C*, *78*, 637.

[9] **Hahn, O. and Paranjape, A.** (2016). General relativistic screening in cosmological simulations, *Phys. Rev. D*, *94*, 083511.

[10] **Canay, E. and Eingorn, M.** (2020). Duel of cosmological screening lengths, *Phys. Dark Univ.*, *29*, 100565.

[11] **Canay, E., Eingorn, M., McLaughlin II, A., Arapoğlu, A.S. and Zhuk, A.** (2022). Effect of peculiar velocities of inhomogeneities on the shape of gravitational potential in spatially curved universe, *Phys. Lett. B*, *831*, 137175.

[12] **Eingorn, M., Canay, E., Metcalf, J.M., Brlinekov, M. and Zhuk, A.** (2021). Effect of the cubic torus topology on cosmological perturbations, *Universe*, *7(12)*, 469.

[13] **Eingorn, M., McLaughlin II, A., Canay, E., Brilenkov, M. and Zhuk, A.** (2021). Gravitational Interaction in the Chimney Lattice Universe, *Universe*, *7(4)*, 101.

[14] **Eingorn, M., McLaughlin II, A., Canay, E., Brilenkov, M. and Zhuk, A.** (2021). Gravitation in the Space with Chimney Topology, *Phys. Sci. Forum*, *2(1)*, 32.

[15] **Springel, V., Pakmor, R., Zier, O. and Reinecke, M.** (2021). Simulating cosmic structure formation with the GADGET-4 code, *Mon. Not. R. Astron. Soc.*, *506*, 2871.

[16] **Dolag, K., Borgani, S., Schindler, S., Diaferio, A. and Bykov, A.M.** (2008). Simulation techniques for cosmological simulations, *SSRv*, *134*, 229.

[17] **Bagla, J.S.** (2005). Cosmological N-body simulation: techniques, scope and status, *Curr. Sci.*, *88*, 1088.

[18] **Marcos, B., Baertschiger, T., Joyce, M., Gabrielli, A. and Labini, F.S.** (2006). Linear perturbative theory of the discrete cosmological N-body problem, *Phys. Rev. D*, *73*, 103507.

[19] **Bailin, D. and Love, A.** (1987). Kaluza-Klein theories, *Rep. Prog. Phys.*, *50*, 1087.

[20] **Overduin, J.M. and Wesson, P.S.** (1997). Kaluza-Klein Gravity, *Phys. Rept.*, *283*, 303.

[21] **Sotiriou, T.P. and Faraoni, V.** (2010). $f(R)$ Theories of Gravity, *Rev. Mod. Phys.*, *82*, 451.

[22] **De Felice, A. and Tsujikawa, S.** (2010). $f(R)$ theories, *Living Rev. Relativ.*, *13*, 3.

[23] **Capozziello, S. and De Laurentis, M.** (2011). Extended Theories of Gravity, *Phys. Rept.*, *509*, 167.

[24] **Nojiri, S. and Odintsov, S.D.** (2011). Unified cosmic history in modified gravity: from $F(R)$ theory to Lorentz noninvariant models, *Phys. Rept.*, *505*, 59.

[25] **Clifton, T., Ferreira, P.G., Padilla, A. and Skordis,C.** (2012). Modified gravity and cosmology, *Phys. Rept.*, *513*, 1.

[26] **Nojiri, S., Odintsov, S.D. and Oikonomou, V.K.** (2017). Modified gravity theories on a nutshell: Inflation, bounce and late-time evolution, *Phys. Rept.*, *692*, 1.

[27] **Eingorn, M. and Zhuk, A.** (2011). Weak-field limit of $f(R)$-gravity in three and more spatial dimensions, *Phys. Rev. D*, *84*, 024023.

[28] **Eingorn, M. and Zhuk, A.** (2012). Asymptotic latent solitons, black strings and black branes in $f(R)$-gravity, *Phys. Rev. D*, *85*, 064030.

[29] **Chopovsky, A., Eingorn, M. and Zhuk, A.** (2012). Weak-field limit of Kaluza-Klein models with spherical compactification: experimental constraints, *Phys. Rev. D*, *85*, 064028.

[30] **Chopovsky, A., Eingorn, M. and Zhuk, A.** (2012). Exact and asymptotic black branes with spherical compactification, *Phys. Rev. D*, *86*, 024025.

[31] **Eingorn, M., Fakhr, S.H. and Zhuk, A.** (2013). Kaluza-Klein models with spherical compactification: observational constraints and possible examples, *Class. Quantum Grav.*, *30*, 115004.

[32] **Faraoni, V. and Lanahan-Tremblay, N.** (2008). Comment on "Solar System constraints to general $f(R)$ gravity", *Phys. Rev. D*, *77*, 108501.

[33] **Faraoni, V.** (2009). Scalar field mass in generalized gravity, *Class. Quantum Grav.*, *26*, 145014.

[34] **Günther, U. and Zhuk, A.** (1997). Gravitational excitons from extra dimensions, *Phys. Rev. D*, *56*, 6391.

[35] **Arkani-Hamed, N., Dimopoulos, S. and March-Russell, J.** (2001). Stabilization of submillimeter dimensions: the new guise of the hierarchy problem, *Phys. Rev. D*, *63*, 064020.

[36] **Kapner, D.J., Cook, T.S., Adelberger, E.G., Gundlach, J.H., Heckel, B.R., Hoyle, C.D. and Swanson, H.E.** (2007). Tests of the Gravitational Inverse-Square Law below the Dark-Energy Length Scale, *Phys. Rev. Lett.*, *98*, 021101.

[37] **Eingorn, M. and Zhuk, A.** (2010). Classical tests of multidimensional gravity: negative result, *Class. Quantum Grav.*, *27*, 205014.

[38] **Landau, L.D. and Lifshitz, E.M.** (2000). *Course of Theoretical Physics Series, Vol. 2, The Classical Theory of Fields*, Oxford Pergamon Press, Oxford.

[39] **Will, C.M.** (1993). *Theory and Experiment in Gravitational Physics*, Cambridge University Press, Cambridge.

[40] **Will, C.M.** (2014). The Confrontation between General Relativity and Experiment, *Living Rev. Relativ.*, *17*, 4.

[41] **Chopovsky, A., Eingorn, M. and Zhuk, A.** (2014). Problematic aspects of Kaluza-Klein excitations in multidimensional models with Einstein internal spaces, *Phys. Lett. B*, *736*, 329.

[42] **Akarsu, Ö., Chopovsky, A. and Zhuk, A.** (2018). Black branes and black strings in the astrophysical and cosmological context, *Phys. Lett. B*, *778*, 190.

[43] **Peacock, J.A.** (1998). *Cosmological Physics*, Cambridge University Press, Cambridge.

[44] **Durrer, R.** (2020). *The Cosmic Microwave Background*, 2nd ed., Cambridge University Press, Cambridge.

[45] **Li, M.-H. and Lin, H.-N** (2015). Testing the homogeneity of the Universe using gamma-ray bursts, *Astron. Astrophys.*, *582*, A111.

[46] **Yadav, J., Bharadwaj, S., Pandey, B. and Seshadri, T.R.** (2005). Testing homogeneity on large scales in the Sloan Digital Sky Survey Data Release One, *Mon. Not. R. Astron. Soc.*, *364*, 601.

[47] **Sarkar, P., Yadav, J., Pandey, B. and Bharadwaj, S.** (2009). The scale of homogeneity of the galaxy distribution in SDSS DR6, *Mon. Not. R. Astron. Soc.*, *399*, L128.

[48] **Scrimgeour, M.I., Davis, T., Blake, C., James, J.B., Poole, G.B., Staveley-Smith, L., ... and Yee, H.K.C.** (2012). The WiggleZ Dark Energy Survey: the transition to large-scale cosmic homogeneity, *Mon. Not. R. Astron. Soc.*, *425*, 116.

[49] **Mukhanov, V.F., Feldman, H.A. and Brandenberger, R.H.** (1992). Theory of cosmological perturbations, *Phys. Rept.*, *215*, 203.

[50] **Bernardeau, F., Colombi, S., Gaztanaga, E. and Scoccimarro, R.** (2002). Largescale structure of the Universe and cosmological perturbation theory, *Phys. Rept.*, *367*, 1.

[51] **Kurki-Suonio, H.** (2022). *Lecture Notes on Cosmological Perturbation Theory I*, 1.6.2022 version, Helsinki.

[52] **Bardeen, J. M.** (1980). Gauge-invariant cosmological perturbations, *Phys. Rev. D*, *22*, 1882.

[53] **Kodama, H. and Sasaki, M.** (1984). Cosmological Perturbation Theory, *Prog. Theo. Phys. Suppl.*, *78*, 1.

[54] **Bertschinger, E.** (1995). Cosmological Dynamics, *arXiv e-prints*, arXiv:astro–ph/9503125.

[55] **Carroll, S.M.** (2019). *Spacetime and Geometry: An Introduction to General Relativity*, Cambridge University Press, Cambridge.

[56] **Baumann, D.** (2014). *Lecture Notes on Cosmology, Part III Mathematical Tripos* , Cambridge.

[57] **Eingorn, M. and Zhuk, A.** (2012). Hubble flows and gravitational potentials in observable Universe, *J. Cosmol. Astropart. Phys.*, *09*, 026.

[58] **Eingorn, M. and Zhuk, A.** (2014). Remarks on mechanical approach to observable Universe, *J. Cosmol. Astropart. Phys.*, *05*, 024.

[59] **Ade, P.A.R, Aghanim, N., Arnaud, M., Ashdown, M., Aumont, J., Baccigalupi, C., ... and Zonca, A. [Planck Collaboration]** (2016). Planck 2015 results XIII. Cosmological parameters, *Astron. Astrophys.*, *594*, A13.

[60] **Aghanim, N., Akrami., Y., Ashdown, M., Aumont, J., Baccigalupi, C., Ballardini, M., ... and Zonca, A. [Planck Collaboration]** (2020). Planck 2018 results VI. Cosmological parameters, *Astron. Astrophys.*, *641*, A6.

[61] **Horvath, I., Hakkila, J. and Bagoly, Z.** (2014). Possible structure in the GRB sky distribution at redshift two, *Astron. Astrophys.*, *561*, L12.

[62] **Horvath, I., Bagoly, Z., Hakkila, J. and Toth, L.V.** (2015). New data support the existence of the Hercules-Corona Borealis Great Wall, *Astron. Astrophys.*, *584*, A48.

[63] **Cornish, N.J., Spergel, D. and Starkman, G.** (1998). Finding topology with the Microwave Background Radiation, *Class. Quantum Grav.*, *15*, 2657.

[64] **Cornish, N.J., Spergel, D.N., Starkman, G.D. and Komatsu, E.** (2004). Constraining the topology of the Universe, *Phys. Rev. Lett.*, *92*, 201302.

[65] **Key, J.S., Cornish, N.J., Spergel, D.N. and Starkman, G.D.** (2007). Extending the WMAP bound on the size of the Universe, *Phys. Rev. D*, *75*, 084034.

[66] **Aurich, R., Lustig, S. and Steiner, F.** (2006). The circles-in-the-sky signature for three spherical universes, *Mon. Not. R. Astron. Soc.*, *369*, 240.

[67] **Mota, B., Reboucas, M.J. and Tavakol, R.** (2010). Circles-in-the-sky searches and observable cosmic topology in a flat Universe, *Phys. Rev. D*, *81*, 103516.

[68] **Mota, B., Reboucas, M.J. and Tavakol, R.** (2011). What can the detection of a single pair of circles-in-the-sky tell us about the geometry and topology of the Universe?, *Phys. Rev. D*, *84*, 083507.

[69] **Luminet, J.-P.** (2008). The shape and topology of the Universe, *arXiv e-prints*, arXiv:0802.2236.

[70] **Aslanyan, G.and Manohar, A.V.** (2012). The topology and size of the Universe from the Cosmic Microwave Background, *J. Cosmol. Astropart. Phys.*, *06*, 003.

[71] **Weisstein, E.W.** "Erfc." From *MathWorld*, A Wolfram Web Resource. Retrieved from https://mathworld.wolfram.com/Erfc.html.

[72] **Klessen, R.** (1997). GRAPESPH with fully periodic boundary conditions: fragmentation of molecular clouds, *Mon. Not. R. Astron. Soc.*, *292*, 11.

[73] **Hernquist, L., Bouchet, F.R. and Suto, Y.** (1991). Application of the Ewald Method to Cosmological N-Body Simulations, *Astrophys. J. Suppl.*, *75*, 231.

[74] **Salin, G. and Caillol, J.-M.** (2000). Ewald sums for Yukawa potentials, *J. Chem. Phys.*, *113*, 10459.

[75] **Ade, P.A.R, Aghanim, N., Arnaud, M., Ashdown, M., Aumont, J., Baccigalupi, C., ... and Zonca, A. [Planck Collaboration]** (2016). Planck 2015 results. XVIII. Background geometry and topology, *Astron. Astrophys.*, *594*, A18.

[76] **Canay, E. and Eingorn, M.** (2022). Yukawa vs. Newton: gravitational forces in a cubic cosmological simulation box, *Eur .Phys. J. Plus*, *137*, 397.

[77] **Kamenshchik, A., Moschella, U. and Pasquier, V.** (2001). An Alternative to quintessence, *Phys. Lett. B*, *511*, 265.

[78] **Bilic, N., Tupper, G.B. and Viollier, R.D.** (2002). Unification of dark matter and dark energy: the inhomogeneous Chaplygin gas, *Phys. Lett. B*, *535*, 17.

[79] **Bento, M.C., Bertolami, O. and Sen, A.A.** (2002). Chaplygin gas, accelerated expansion, and dark-energy matter unification, *Phys. Rev. D*, *66*, 043507.

[80] **Benaoum, H.B.** (2022). Accelerated Universe from modified Chaplygin gas and tachyonic fluid, *Universe*, *8(7)*, 340.

[81] **Baumann, D., Nicolis, A., Senatore, L. and Zaldarriaga, M.** (2012). Cosmological non-linearities as an effective fluid, *J. Cosmol. Astropart. Phys.*, *07*, 051.

[82] **Eingorn, M., and Zhuk, A.** (2011). Kaluza-Klein models: can we construct a viable example?, *Phys. Rev. D*, *83*, 044005.

[83] **Eingorn, M., de Medeiros, O., Crispino, L. and Zhuk, A.** (2011). Latent solitons, black strings, black branes, and equations of state in Kaluza-Klein models, *Phys. Rev. D*, *84*, 024031.

[84] **Eingorn, M. and Zhuk, A.** (2012). Remarks on gravitational interaction in Kaluza-Klein models, *Phys. Lett. B*, *713*, 154.

[85] **Eingorn, M. and Zhuk, A.** (2010). Non-relativistic limit of multidimensional gravity: exact solutions and applications, *Class. Quantum Grav.*, *27*, 055002.

[86] **Canay, E., Eingorn, M. and Zhuk, A.** (2020). Effects of nonlinearity of $f(R)$ gravity and perfect fluid in Kaluza-Klein models with spherical compactification, *Eur .Phys. J. C*, *80*, 379.

[87] **Yadav, J.K., Bagla, J.S., Khandai, N.** (2010). Fractal dimension as a measure of the scale of homogeneity, *Mon. Not. R. Astron. Soc.*, *405*, 2009.

[88] **Eingorn, M., Yukselci, A.E. and Zhuk, A.** (2022). Screening vs. gevolution: in chase of a perfect cosmological simulation code, *Phys. Lett. B*, *826*, 136911.

[89] **Brilenkov, R. and Eingorn, M.** (2017). Second-order Cosmological Perturbations Engendered by Point-like Masses, *Astrophys. J.*, *845*, 153.

[90] **Eingorn, M., Guran, N.D. and Zhuk, A.** (2019). Analytic expressions for the second-order scalar perturbations in the ΛCDM Universe within the cosmic screening approach, *Phys. Dark Univ.*, *26*, 100329.

[91] **Räsänen, S.** (2011). Backreaction: directions of progress, *Class. Quant. Grav.*, *28*, 164008.

[92] **Clarkson, C., Ellis, G., Larena, J. and Umeh, O.** (2011). Does the growth of structure affect our dynamical models of the universe? The averaging, backreaction and fitting problems in cosmology, *Rept. Prog. Phys.*, *74*, 112901.

[93] **Buchert, T. and Räsänen, S.** (2012). Backreaction in late-time cosmology, *Annual Review of Nuclear and Particle Science*, *62*, 57.

[94] **Green, S.R. and Wald, R.M.** (2013). Examples of backreaction of small scale inhomogeneities in cosmology, *Phys. Rev. D*, *87*, 124037.

[95] **Bolejko, K. and Korzyński, M.** (2017). Inhomogeneous cosmology and backreaction: Current status and future prospects, *Int. J. Mod. Phys. D*, *26*, 1730011.

CURRICULUM VITAE

Name Surname: Ezgi Yılmaz

EDUCATION:

- **BSc:** July 2013, Istanbul Technical University, Faculty of Science and Letters, Department of Physics
- **MSc:** June 2018, Istanbul Technical University, Faculty of Science and Letters, Department of Physics

PROFESSIONAL EXPERIENCE AND REWARDS:

- 2017 - 2022 Research Assistant at the Department of Physics, Istanbul Technical University.
- 2013 - 2014 Graduate Teaching Assistant at the Faculty of Engineering and Natural Sciences, Sabancı University

PUBLICATIONS AND PRESENTATIONS ON THE THESIS:

- **Canay, E.,** Eingorn, M., McLaughlin II, A., Arapoğlu, A.S. and Zhuk, A. (2022). Effect of peculiar velocities of inhomogeneities on the shape of gravitational potential in spatially curved universe, *Phys. Lett. B*, *831*, 137175.
- **Canay, E.** and Eingorn, M., (2022). Yukawa vs. Newton: gravitational forces in a cubic cosmological simulation box, *Eur. Phys. J. Plus*, *137*, 397.
- **Canay, E.,** Brilenkov, R., Eingorn, M., Arapoğlu, A.S. and Zhuk, A. (2021). Scalar and vector perturbations in a universe with nonlinear perfect fluid, *Eur. Pyhs. J. C*, *81*, 246.
- **Canay, E.** and Eingorn, M., (2020). Duel of cosmological screening lengths, *Phys. Dark Univ.*, *29*, 100565.
- **Canay, E.,** Eingorn, M. and Zhuk, A., (2020). Effects of nonlinearity of $f(R)$ gravity and perfect fluid in Kaluza–Klein models with spherical compactification, *Eur. Pyhs. J. C*, *80*, 379.

OTHER PUBLICATIONS AND PRESENTATIONS:

- Eingorn, M., **Canay, E.,** Metcalf, J.M., Brilenkov, M. and Zhuk, A. (2021). Effect of the cubic torus topology on cosmological perturbations, *Universe*, *7(12)*, 469.

- Eingorn, M., McLaughlin II, A., **Canay, E.,** Brilenkov, M. and Zhuk, A. (2021). Gravitational Interaction in the Chimney Lattice Universe, *Universe*, *7(4)*, 101.
- Eingorn, M., McLaughlin II, A., **Canay, E.,** Brilenkov, M. and Zhuk, A. (2021). Gravitation in the Space with Chimney Topology, *Phys. Sci. Forum*, *2(1)*, 32.
- Akarsu, Ö., Chopovsky, A., Shulga, V., **Yalçınkaya, E.,** and Zhuk, A. (2020). Weak field limit of higher dimensional massive Brans-Dicke gravity: Observational constraints, *Phys. Rev. D*, *101*, 024004.
- **Yalçınkaya, E.,** and Zhuk, A. (2019). Weak-Field Limit of a Kaluza-Klein Model with a Nonlinear Perfect Fluid, *Grav. Cosmol.*, *25*, 349.
- Arapoğlu, A.S. **Canay, E.,** and Yükselci, A.E. (2018). Dynamical system analysis of a five-dimensional cosmological model, *Astrophys. Space Sci.*, *363*, 215.